Majorana scars as group singlets

Zimo Sun [1], Fedor K. Popov,[2] Igor R. Klebanov [1,3] and Kiryl Pakrouski [4]

[1]*Department of Physics, Princeton University, Princeton, New Jersey 08544, USA*
[2]*Department of Physics, New York University, New York, New York 10003, USA*
[3]*Princeton Center for Theoretical Science, Princeton University, Princeton, New Jersey 08544, USA*
[4]*Institute for Theoretical Physics, ETH Zurich, 8093 Zurich, Switzerland*

In some quantum many-body systems, the Hilbert space breaks up into a large ergodic sector and a much smaller scar subspace. It has been suggested [K. Pakrouski *et al.*, Phys. Rev. Lett. **125**, 230602 (2020)] that the two sectors may be distinguished by their transformation properties under a large group whose rank grows with the system size (it is not a symmetry of the Hamiltonian). The quantum many-body scars are invariant under this group, while all other states are not. Here we apply this idea to lattice systems containing M Majorana fermions per site. The Hilbert space for N sites may be decomposed under the action of the $SO(N) \times SO(M)$ group, and the scars are the $SO(N)$ singlets. For any even M there are two families of scars. One of them, which we call the η states, is symmetric under the group $O(N)$. The other, the ζ states, has the $SO(N)$ invariance. For $M = 4$, where our construction reduces to spin-1/2 fermions on a lattice with local interactions, the former family are the $N + 1$ η-pairing states, while the latter are the $N + 1$ states of maximum spin. We generalize this construction to $M > 4$. For $M = 6$ we exhibit explicit formulas for the scar states and use them to calculate the bipartite entanglement entropy analytically. For large N, it grows logarithmically with the subsystem size. We present a general argument that any group-invariant scars should have the entanglement entropy that is parametrically smaller than that of typical states. The energies of the scars we find are not equidistant in general but can be made so by choosing Hamiltonian parameters. For $M > 6$ we find that with local Hamiltonians the scars typically have certain degeneracies. The scar spectrum can be made ergodic by adding a nonlocal interaction term. We derive the dimension of each scar family and show the scars could have a large contribution to the density of states for small N.

I. INTRODUCTION

The past few years have seen growing interest in "quantum many-body scars," the term that was coined in Ref. [1]. The essential phenomenon is that there are many-body systems where the Hilbert space breaks up into the bulk of states that satisfy the eigenstate thermalization hypothesis (ETH), and a much smaller scar subspace that does not. Specific constructions of such states have been found in a variety of models [1–48]. For the recent reviews of the different approaches to scars, see Refs. [49–52]. A related phenomenon of nonstationary dynamics has also been identified in open systems [48,53].

Remarkably, the quantum many-body scars appear in the commonly used models of condensed matter physics, such as the (deformed) Fermi-Hubbard and t-J-U models on a lattice with N sites. Such models contain two species of complex fermions on each site, $c_{j\uparrow}$ and $c_{j\downarrow}$. In addition to the rotational SU(2) symmetry, they possesses a (broken) pseudospin $\widetilde{SU}(2)$ symmetry. The η-pairing states [54,55] form a multiplet of

pseudospin $N/2$, and their role as scars was pointed out and studied in Refs. [14,20,22,32]. Another important family are the ζ states that carry the maximum spin $N/2$; they can be regarded as scars if the SU(2) rotational symmetry is broken [22,32].

There has also been important progress on. generalizing the η-pairing states to systems with more than two complex fermions per lattice site [38,43] (for earlier work, see also Ref. [56]).

In this paper we present a systematic method for constructing multiflavor fermionic systems with weak ergodicity breaking (many-body scars) that leads to generalizing the η and ζ states. It relies on the idea that the scar subspace is invariant under a "large group" whose rank is of the order of the number of lattice sites N [22,32]. Indeed, the η-pairing scars in the spin-1/2 Hubbard model have been shown to be invariant under SO(N) which acts on the lattice site index [22], as well as under an even bigger symplectic group $\widetilde{Sp}(N)$ [32].

We consider lattice systems of arbitrary dimension with an even number M of Majorana fermions per lattice site and rely on the method proposed in Ref. [22]: The many-body scars span a subspace of the Hilbert space invariant under a large group G that is *not* a symmetry of the system. The Hamiltonian is chosen to be of the form $H = H_0 + \sum_a \mathcal{O}_a T_a$,

where H_0 is a term governing the dynamics of the scar subspace, T_a are generators of the group G, which therefore annihilate the scars, and $\mathcal{O}_a$ are operators chosen so that the Hamiltonian is Hermitian. Here we apply this construction using the group $G = \mathrm{SO}(N)$ and H_0 given by the (generalized) Hubbard model, which commutes with the quadratic Casimir operator of $\mathrm{SO}(N)$. We also exhibit other operators that can be used as building blocks of scarred Hamiltonians in this Hilbert space, thus providing a toolbox for future studies.

Our system is equivalent to $M/2$ complex fermions per site, and for $M = 4$ we reproduce the previous results singling out $N + 1$ η states and $N + 1\zeta$ states as the scars. For $M = 6$ we present concise formulas for all the $\mathrm{SO}(N)$ singlets, which come in two families generalizing the η and ζ states. The expressions for the generalized η states are the same as those found in Ref. [43], where it was also understood that they are eigenstates of the $\mathrm{SU}(3)$-invariant Hubbard interaction. We calculate the bipartite entanglement entropy for $M = 6$ analytically. For small N we confirm numerically that the invariant states we consider possess all the characteristic properties of many-body scars. In particular their entanglement entropy is found to be much smaller than that of the nearby thermal states. For large N we show analytically that the entanglement entropies of scars grows logarithmically with the region size for any M.

Practically all the many-body scars known in literature are characterized by the lower entanglement entropy compared to generic states in the same energy range. This feature is even sometimes included into the definition of scars. However, the underlying mechanism behind this has remained unclear. Generalizing our results for the Majorana scars we present in Sec. V a general argument that any group-invariant scars in any system built according to the group-invariant formalism [22] must have a parametrically lower entanglement and conjecture that the entropy of other, not group-invariant scars is reduced for a similar reason.

For $M > 4$, the scars within the η and ζ families are not in general equidistant in energy even if the Hamiltonian is restricted to local terms only. We discuss the conditions under which the "revivals" can nevertheless be observed. Because of the large number of scars (this is also the case in the model of [57]), their presence is noticeable in the density of states for small N, which has implications for their experimental detection. Furthermore, the scar spectrum becomes ergodic if the H_0 part [22] of the Hamiltonian is chosen to be nonintegrable. These features of many-body scar spectrum are reported here for the first time to our knowledge.

For $M > 6$ the $\mathrm{SU}(M/2)$-invariant Hubbard interaction no longer works simply. Therefore, we replace it by another local interaction under which all the $\mathrm{SO}(N)$ singlets are eigenstates. A novel feature we find for the scar states with $M > 6$ is the presence of degeneracies which appear to be protected from any local interactions, but can be broken by nonlocal ones.

II. DEFORMED HUBBARD MODEL AND SCARS

In this section, we review the $\mathrm{SO}(4)$ symmetry of the Hubbard model, using both Dirac and Majorana fermions,

and discuss its relation with the scar states in some deformed Hubbard models. For simplicity of the discussion, we consider here the model on a one-dimensional (1D) lattice of N sites but the results hold [32] in any dimension. The standard Hubbard Hamiltonian is the sum of three terms—the hopping, the on-site repulsion, and the chemical potential:

$$
T = -t \sum_{j=1}^{N-1} \sum_{\sigma \in \{\uparrow, \downarrow\}} (c_{j\sigma}^\dagger c_{j+1,\sigma} + c_{j+1,\sigma}^\dagger c_{j\sigma}),
$$

$$
V = U \sum_{j=1}^{N} n_{j\uparrow} n_{j\downarrow} = U \sum_{j=1}^{N} c_{j\uparrow}^\dagger c_{j\uparrow} c_{j\downarrow}^\dagger c_{j\downarrow},
$$

$$
\mu = -\sum_{j=1}^{N} (\mu_\downarrow c_{j\downarrow}^\dagger c_{j\downarrow} + \mu_\uparrow c_{j\uparrow}^\dagger c_{j\uparrow}). \tag{1}
$$

Here t is a real hopping parameter, $U > 0$ is the on-site interaction strength, and $c_{i\sigma}, c_{i\sigma}^\dagger$ are the fermionic ladder operators satisfying the anticommutation relations

$$
\{c_{i\sigma}, c_{j\sigma'}^\dagger\} = \delta_{ij} \delta_{\sigma\sigma'} . \tag{2}
$$

The magnetic field is $(\mu_\uparrow - \mu_\downarrow)/2$ while the standard chemical potential is $(\mu_\uparrow + \mu_\downarrow)/2$. We find it convenient to perform a site dependent phase rotation, $c_{j\sigma} \to e^{-ij\frac{\pi}{2}} c_{j\sigma}$, on which the hopping term acquires an imaginary coefficient,

$$
T' = it \sum_{j=1}^{N-1} \sum_{\sigma \in \{\uparrow, \downarrow\}} (c_{j\sigma}^\dagger c_{j+1,\sigma} - c_{j+1,\sigma}^\dagger c_{j\sigma}), \tag{3}
$$

In these variables, the Hubbard Hamiltonian is $H_{\mathrm{Hub}} = T' + V + \mu$. This transformation could be performed on any dimensional bipartite lattice [32]. We shall not restrict ourselves only to bipartite lattices and consider the Hamiltonian (3) on any lattice.

The time-reversal symmetry in this case is defined as follows:

$$
\mathrm{T} c_{i\uparrow} \mathrm{T}^{-1} = (-1)^i c_{i\downarrow}, \quad \mathrm{T} c_{i\downarrow} \mathrm{T}^{-1} = (-1)^{i+1} c_{i\uparrow}. \tag{4}
$$

For the vanishing magnetic field, $\mu_\uparrow = \mu_\downarrow$, the Hamiltonian H_{Hub} has both time-reversal symmetry and the spin $\mathrm{SU}(2)$ symmetry, which acts on the spin index σ. The generators of $\mathrm{SU}(2)$ are

$$
\zeta_3 = \frac{1}{2} \sum_j (c_{j\uparrow}^\dagger c_{j\uparrow} - c_{j\downarrow}^\dagger c_{j\downarrow}),
$$

$$
\zeta^+ = \sum_j c_{j\uparrow}^\dagger c_{j\downarrow}, \quad \zeta^- = \sum_j c_{j\downarrow}^\dagger c_{j\uparrow}. \tag{5}
$$

When $\mu_\uparrow = \mu_\downarrow = \frac{U}{2}$, the $\mathrm{SU}(2)$ symmetry is enhanced to $\mathrm{SO}(4) = \mathrm{SU}(2) \times \widetilde{\mathrm{SU}}(2)/\mathbb{Z}_2$, where the pseudospin group $\widetilde{\mathrm{SU}}(2)$ is generated by [54,55,58]

$$
\eta_3 = \frac{1}{2} \sum_j \sum_\sigma c_{j\sigma}^\dagger c_{j\sigma} - \frac{N}{2},
$$

$$
\eta^+ = \sum_j c_{j\uparrow}^\dagger c_{j\downarrow}^\dagger, \quad \eta^- = \sum_j c_{j\downarrow} c_{j\uparrow}, \tag{6}
$$

and the $\mathbb{Z}_2$ factor is realized by the Shiba transformation [32,59,60]. The SO(4) symmetry becomes manifest if we use a Majorana representation of the Dirac spinors $c_{j\sigma}$. Namely, we define

$$c_{j\uparrow} = \frac{\psi_j^1 - i\psi_j^2}{\sqrt{2}}, \quad c_{j\downarrow} = \frac{\psi_j^3 - i\psi_j^4}{\sqrt{2}}, \qquad (7)$$

where ψ_j^A, $A = 1, 2, 3, 4$ are four Majorana fermions on site j. Then H_{Hub} at $\mu_\uparrow = \mu_\downarrow = \frac{U}{2}$ admits a manifestly SO(4)-invariant form,

$$H_{\text{Hub}} = it \sum_j \sum_{A=1}^4 \psi_j^A \psi_{j+1}^A - U \sum_j \psi_j^1 \psi_j^2 \psi_j^3 \psi_j^4 - \frac{UN}{4}, \qquad (8)$$

where the hopping terms $\sum_A \psi_j^A \psi_{j+1}^A$ can be identified as special cases of the (anti-Hermitian) SO(N) generators $T_{jk} \equiv \sum_A \psi_j^A \psi_k^A$, $1 \leqslant j < k \leqslant N$. The SO($N$) group acts on the site indices of Majorana fermions, i.e., $\psi_j^A \to R_{ij} \psi_j^A$, where R_{ij} is a special orthogonal matrix. The SO(N) singlet subspace consists of η states,

$$|m^\eta\rangle \equiv \frac{(\eta^+)^m}{\sqrt{\frac{N!m!}{(N-m)!}}} |0^\eta\rangle, \quad m = 0, 1, 2, \ldots, N, \qquad (9)$$

where the η vacuum $|0^\eta\rangle$ is the same as the empty vacuum $|0\rangle$, and the ζ states

$$|m^\zeta\rangle \equiv \frac{(\zeta^+)^m}{\sqrt{\frac{N!m!}{(N-m)!}}} |0^\zeta\rangle, \quad m = 0, 1, 2, \ldots, N, \qquad (10)$$

where the ζ vacuum is $|0^\zeta\rangle \equiv c_{1\downarrow}^\dagger \cdots c_{N\downarrow}^\dagger |0\rangle$. The η states span an $(N+1)$-dimensional representation of the pseudospin group $\widetilde{\text{SU}}(2)$ and the ζ states furnish a spin $\frac{N}{2}$ representation of the spin group SU(2). The ζ states have fixed fermion number N and have eigenenergies $-(\mu_\uparrow - \mu_\downarrow)m - \mu_\downarrow N$ with respect to the Hubbard Hamiltonian H_{Hub}. The η states are also energy eigenstates of the Hubbard Hamiltonian, i.e., $H_{\text{Hub}}|m^\eta\rangle = m(U - \mu_\downarrow - \mu_\uparrow)|m^\eta\rangle$. In Ref. [32], the authors constructed the Hubbard model deformed by quartic OT terms that break both the spin and pseudospin symmetries. Then the SO(N)-invariant η and ζ states remain eigenstates, and they have all the typical properties of scar states. In the next section we will consider a different set of symmetry breaking deformations which also keep the η and ζ states as scars. We will also extend the construction from four Majorana fermions per site to a higher even number M.

III. MULTIFLAVOR MAJORANA FERMIONS ON A LATTICE

Generalizing the Majorana description of the Hubbard model, we consider a lattice of N sites, hosting an even number M flavors of Majorana fermions ψ_j^A, $A = 1, 2, \ldots, M$ on each site. Their anticommutation relations,

$$\{\psi_i^A, \psi_j^B\} = \delta^{AB} \delta_{ij}, \qquad (11)$$

are invariant under the action of SO(N) × SO(M) group. We can build (anti-Hermitian) generators of SO(N) and SO(M) from these fermions,

$$T_{ij} = \frac{1}{2} \sum_{A=1}^M [\psi_i^A, \psi_j^A], \quad J^{AB} = \frac{1}{2} \sum_{j=1}^N [\psi_j^A, \psi_j^B]. \qquad (12)$$

Their commutation relations are given by

$$[T_{ij}, T_{kl}] = \delta_{jk} T_{il} - \delta_{ik} T_{jl} - \delta_{jl} T_{ik} + \delta_{il} T_{jk}$$
$$[J^{AB}, J^{CD}] = \delta^{BC} J^{AD} - \delta^{AC} J^{BD} - \delta^{BD} J^{AC} + \delta^{AD} J^{BC}$$
$$[T_{ij}, J^{AB}] = 0. \qquad (13)$$

Grouping the Majorana fermions into complex combinations provides a convenient way to construct states in the Hilbert space. On each site j, define $\alpha = 1, \ldots, M/2$ flavors of complex fermions

$$c_{j\alpha} = \frac{\psi_j^{2\alpha-1} - i\psi_j^{2\alpha}}{\sqrt{2}}, \quad c_{j\alpha}^\dagger = \frac{\psi_j^{2\alpha-1} + i\psi_j^{2\alpha}}{\sqrt{2}}, \qquad (14)$$

which satisfy the standard anticommutation relations $\{c_{i\alpha}, c_{j\beta}^\dagger\} = \delta_{\alpha\beta}\delta_{ij}$. Following the general recipe described in Appendix A, we construct a basis of $\mathfrak{so}(M)$ in terms of these complex fermions that makes its root decomposition structure manifest:

Cartan generators: $h_\alpha = \sum_j c_{j\alpha}^\dagger c_{j\alpha} - \frac{N}{2}$

Raising operators: $\zeta_{\beta\gamma}^\dagger = \sum_j c_{j\beta}^\dagger c_{j\gamma}, \quad \eta_{\beta\gamma}^\dagger = \sum_j c_{j\beta}^\dagger c_{j\gamma}^\dagger$

Lowering operators: $\zeta_{\beta\gamma} = \sum_j c_{j\gamma}^\dagger c_{j\beta}, \quad \eta_{\beta\gamma} = \sum_j c_{j\gamma} c_{j\beta},$

$$(15)$$

where $1 \leqslant \beta < \gamma \leqslant M/2$. The Cartan generators h_α count fermion numbers of each flavor α (up to the constant shift $-\frac{N}{2}$), and the raising and lowering operators hop the fermions in a particular direction (in the flavor space). They correspond to the positive and negative roots of $\mathfrak{so}(M)$ (defined in Appendix A), respectively.

The full Hilbert space $\mathcal{H}$ has dimension $2^{MN/2}$ and forms a spinor representation of the group SO(MN) which acts on the collective index $I = (A; i)$. The decomposition of $\mathcal{H}$ under the subgroup SO(N) × SO(M) was studied in Refs. [61,62]. The quadratic Casimir operators of SO(N) and SO(M), defined by Eq. (A2), satisfy the sum rule [61]

$$\mathcal{C}_2^{\text{SO}(N)} + \mathcal{C}_2^{\text{SO}(M)} = \frac{1}{8} MN(M + N - 2). \qquad (16)$$

In particular, the SO(N) singlets have SO(M) Casimir $\frac{1}{8}MN(M + N - 2)$, which according to Eq. (A7) implies that these singlet states furnish representations of highest weight or their direct sums,

$$\lambda_{N/2}^\pm \equiv \frac{1}{2} \underbrace{(N, N, \cdots, \pm N)}_{M/2}, \qquad (17)$$

where the right-hand side denotes a rectangular Young tableaux with N columns of height $M/2$. When N is even,

it was found in Ref. [62] that the SO(N) singlets furnish the reducible representation $\lambda_{N/2}^+ \oplus \lambda_{N/2}^-$ by using a character method. We will present an elementary way to show that this structure holds for both odd and even N in Sec. IV, where we study in more detail the structure of these singlets.

A. Ergodic Hamiltonians that support singlet states as many-body scars

Following the recipe proposed in Ref. [22], we construct (local) Hamiltonians of the form $H = H_0 + \sum \mathcal{O}_{ij} T_{ij}$. The first term H_0 is designed to leave the space of SO(N) singlets (denoted by $\mathbb{S}$) invariant. The second term, which will be referred to as the OT term henceforth, should be Hermitian and break some symmetries of H_0, by choosing $\mathcal{O}_{ij}$ properly. The Hamiltonians we discuss below should have as few symmetries as possible such that they are guaranteed to produce ergodic bulk spectra and such that the many-body scars are not fully occupying an isolated sector of a symmetry. Nevertheless, the Hamiltonians we consider always preserve the fermion number parity symmetry,

$$P_f = (-1)^Q, \quad Q = \sum_{j=1}^{N} \sum_{\alpha=1}^{M/2} n_{j\alpha}, \quad [P_f, H] = 0, \quad (18)$$

where $n_{j\alpha} = c_{j\alpha}^\dagger c_{j\alpha}$ is the fermion number operator of flavor α at site j. All the numerical computations presented in Sec. VI are performed separately in each of the two sectors.

The Hubbard Hamiltonian in Eq. (8) admits a straightforward SO(M)-invariant generalization to the M-flavor Majorana model on any lattice, namely $H_M \equiv T_M + H_\mu + V_M$, where

$$T_M = it \sum_{\langle j,k \rangle} T_{jk} = it \sum_{\langle j,k \rangle} \sum_{A=1}^{M} \psi_j^A \psi_k^A,$$

$$H_\mu = -\sum_\alpha \mu_\alpha \left(h_\alpha + \frac{N}{2} \right) = -\sum_\alpha \mu_\alpha \sum_j n_{j\alpha},$$

$$V_M = U i^{\frac{M}{2}} \sum_j \psi_j^1 \psi_j^2 \cdots \psi_j^M - 2^{-\frac{M}{2}} NU. \quad (19)$$

The hopping term T_M is summed over nearest neighbors. It can be thought as a special OT term with $\mathcal{O}_{ij} \equiv it$ when (i, j) are nearest neighbors and $\mathcal{O}_{ij} = 0$ otherwise. The V_M term leaves $\mathbb{S}$ invariant because the states in $\mathbb{S}$ have a fixed SO(M) Casimir $\frac{MN}{8}(M + N - 2)$ and V_M commutes with the SO(M) generators. Then the sum rule (16) implies that $V_M \mathbb{S} \subset \mathbb{S}$. Furthermore,

$$\left[H_M, \mathcal{C}_2^{\text{SO}(N)} \right] = 0, \quad (20)$$

which is a special case of the criterion proposed in Eq. (1) of Ref. [22]. This equation means that the Hubbard model, as well as its higher M generalizations (19), factorizes the Hilbert space into the representations of SO(N). SO(N) symmetry is broken in a way that only creates energy splittings within the representations but does not mix different SO(N) representations.

In the complex fermion basis,

$$T_M = it \sum_{\langle j,k \rangle} \sum_\alpha (c_{j\alpha}^\dagger c_{k\alpha} - c_{k\alpha}^\dagger c_{j\alpha}),$$

$$V_M = U \sum_j \prod_\alpha \left(\frac{1}{2} - n_{j\alpha} \right) - 2^{-\frac{M}{2}} NU. \quad (21)$$

The constant shift insures that V_M vanishes when all $n_{j\alpha}$ are equal to zero. For $M = 4$, $T_4 + V_4 + H_\mu$ is equivalent to the standard Hubbard Hamiltonian with chemical potentials $\mu_\uparrow = \mu_1 + \frac{U}{2}$, and $\mu_\downarrow = \mu_2 + \frac{U}{2}$. For general M, since $n_{j\alpha}$ takes value in $\{0, 1\}$, we have $\frac{1}{2} - n_{j\alpha} = \frac{1}{2}(-1)^{n_{j\alpha}}$ and hence V_M can be simplified as

$$V_M = U \sum_j \frac{(-1)^{n_j} - 1}{2^{\frac{M}{2}}}, \quad n_j = \sum_{\alpha=1}^{M/2} n_{j\alpha}, \quad (22)$$

where n_j is the total fermion number at site j.

The chemical potentials in H_μ break the SO(M) symmetry of H_M. In general, to break SO(M), we could start with the more general $\sum_{AB} i\mu_{AB} J^{AB}$, where μ_{AB} is a real antisymmetric matrix, and then redefine the Majorana fermions to get H_μ (up to a constant shift). While H_μ breaks the SO(M) symmetry, the SO(M) Casimir $\mathcal{C}_2^{\text{SO}(M)}$ is still a conserved charge, since all h_α in H_μ commute with $\mathcal{C}_2^{\text{SO}(M)}$.

In the Hubbard model (1), generic chemical potentials $\mu_\uparrow$ and $\mu_\downarrow$ break the SO(4) symmetry. For the Hamiltonian H_M, the Casimir operators of SU(2) and $\widetilde{\text{SU}}(2)$ (consider $M = 4$) are conserved charges because the symmetry breaking term is a linear combination of η_3 and ζ_3. The OT term can be used to break the conservation of $\mathcal{C}_2^{\text{SO}(\widetilde{M})}$. For instance, the following sextic interacting term does this job:

$$\widetilde{H}_{\text{int}} = \sum_{\langle j,k \rangle} T_{jk} \left(i \sum_{A<B} r_{AB} \psi_j^A \psi_j^B \right) T_{jk}, \quad (23)$$

where r_{AB} are randomly chosen real numbers. This form of local interacting Hamiltonian is similar to that adopted by Shiraishi and Mori [3], $\sum_j P_j h_j P_j$, where P_j is a set of local projection operators that satisfy $P_j^2 = P_j$. While our SO(N) generators T_{jk} are not projectors and do not commute, our singlet conditions on the scar states, $T_{jk}|\phi\rangle = 0$ are analogous to the conditions $P_j|\phi\rangle = 0$ imposed in Ref. [3]. In the recent papers [41,42], some parallels were drawn between the approach identifying scars as the sector invariant under a large group [22,32] and the Shiraishi-Mori construction.

Adding up H_M and $\widetilde{H}_{\text{int}}$, we get the following Hamiltonian:

$$H = -\sum_\alpha \mu_\alpha \sum_j n_{j\alpha} + U i^{\frac{M}{2}} \sum_j \psi_j^1 \psi_j^2 \cdots \psi_j^M - 2^{-\frac{M}{2}} NU$$

$$+ it \sum_{\langle j,k \rangle} T_{jk} + \sum_{\langle j,k \rangle} T_{jk} \left(i \sum_{A<B} r_{AB} \psi_j^A \psi_j^B \right) T_{jk}. \quad (24)$$

In terms of the general scheme [22], $H_0 = H_M$ and $H_1 = \widetilde{H}_{\text{int}}$. Later, in Sec. VI A we confirm numerically that the Hamiltonian (24) indeed exhibits weak ergodicity breaking.

Alternatively, instead of the sextic interaction OT term (23), we may consider the quartic one,

$$H_{OT} = i \sum_{\langle j,k \rangle} \mathcal{O}_{jk} T_{jk}, \qquad (25)$$

with $\mathcal{O}_{jk}$ being Hermitian, quadratic in Majorana operators and satisfying $[\mathcal{O}_{jk}, T_{jk}] = 0$. It is easy to check that such H_{OT} is Hermitian and annihilates the singlets. There is a simple way to construct $\mathcal{O}_{jk}$ by noting that T_{jk} can be regarded as a generator of a $U(1)$ Q_T symmetry. This gives the following charges:

$$Q_T(\psi_i^A) = 0, \quad Q_T(d_\pm^{jk,A}) = \pm 1, \quad d_\pm^{jk,A} = \psi_j^A \pm i\psi_k^A.$$

An operator $\mathcal{O}_{jk}$ that has zero charge Q_T then commutes with the hopping operator T_{jk}. For instance, we can consider the following term, that is biliniear in $d_\pm^{jk,A}$:

$$H_{OT} = i \sum_{\langle j,k \rangle} \left(\sum_{AB} R_{AB} d_+^{jk,A} d_-^{jk,B} \right) T_{jk}, \quad R_{AB}^* = R_{BA}. \qquad (26)$$

In Sec. VI B we provide numerical evidence that the Hamiltonian that includes (26) also supports many-body scars.

Another natural generalization of the Hubbard model would be on-site density-density interaction between different flavors, which can be described by the following potential [63]:

$$\widetilde{V}_M = \widetilde{U} \sum_j \sum_{\alpha < \beta} n_{j\alpha} n_{j\beta}. \qquad (27)$$

This term does not have SO(M) symmetry for $M \geqslant 6$ which was also noticed in Ref. [43] although $\widetilde{V}_M$ still keeps some of the scar states considered in Ref. [43] invariant.

B. Controlling the position of scars in the spectrum

One of the possible strategies [32] to control the position of scars in the spectrum relies on the addition of a term that annihilates all the scars but acts positive definitely on all other states. Because scars are SO(N) invariant in our case the most obvious choice for such a term is the quadratic Casimir operator of the SO(N) group,

$$\mathcal{C}_2^{SO(N)} = -\frac{1}{2} \sum_{i=1}^N \sum_{j=1}^N T_{ij}^2, \qquad (28)$$

where T_{ij} are SO(N) generators given in Eq. (12). The interaction in Eq. (28) is, however, highly nonlocal in real space.

We find numerically that for the accessible system sizes also the following local interaction can be used where the summation is only over the nearest neighbors:

$$H_{T^2} = -\sum_{\langle ij \rangle} T_{ij}^2. \qquad (29)$$

It is non-negative definite, and because of the presence of SO(N) generators, we have

$$H_{T^2} |s\rangle = 0, \quad \langle ns|H_{T^2}|ns\rangle > 0, \qquad (30)$$

where $|s\rangle$ is an SO(N) singlet state and $|ns\rangle$ is a nonsinglet state. Therefore, it can be used to change the position of the scars in energy with respect to all other states without

changing the relative position (and the revivals period) of scars themselves. In particular, using Eq. (29) one can achieve that the low-energy part of the spectrum is composed of many-body scars only as shown in Fig. 6.

Another strategy for scar spectrum design is also inspired by the single-band case [32] where the scars furnished the highest-spin representation of SU(2) and would therefore be the most susceptible states to the magnetic field which in turn allows to make a scar the ground state.

Similarly, the scar subspace in the present case corresponds to the highest-weight representation of SO(M) (see Sec. IV A) and includes the states most susceptible to the chemical potential (19) H_μ part of the Hamiltonian. Therefore by a suitable choice of the strong chemical potential (playing here a role of a generalized magnetic field) one can always achieve that a scar state becomes the ground state.

IV. SO(N) SINGLETS AS SCARS

In this section we discuss properties of the SO(N) singlets for arbitrary M. For $M = 6$, i.e., six Majorana fermion flavors per site, we write down the wave function of every SO(N) singlet. Similar explicit formulas for the η states have been obtained in the SU(3) Hubbard model [43]. Furthermore, we show analytically that both the η states and the ζ states have a subvolume law for entanglement entropy in the thermodynamic limit.

A. The SO(M) representation structure of SO(N) singlets

From the Casimir relation (16), we know that the possible SO(M) representation structure of the SO(N) singlets is a direct sum of the maximal-weight representations from Eq. (17):

$$\mathbb{S} = \underbrace{\lambda_{N/2}^+ \oplus \cdots \oplus \lambda_{N/2}^+}_{n_+} \oplus \underbrace{\lambda_{N/2}^- \oplus \cdots \oplus \lambda_{N/2}^-}_{n_-}, \qquad (31)$$

where $n_\pm$ are multiplicities of each $\lambda_{N/2}^\pm$ representation. Given a highest weight representation R, its lowest-weight vector is given by minus of the highest-weight vector of the dual representation R^*. When $n = M/2$ is even, all highest-weight representations of SO($2n$) are self-dual, and when n is odd, the dual representation is given by flipping the sign of the last entry of the highest-weight vector. More explicitly, the lowest-weight vector corresponding to $(\lambda_1, \lambda_2, \ldots, \lambda_n)$ is $(-\lambda_1, -\lambda_2, \ldots, (-)^{n+1}\lambda_n)$. For the two irreducible representations in Eq. (31), the corresponding lowest-weight vectors are $-\frac{1}{2}(N, N, \ldots, \pm N)$.

This implies that the lowest-weight states have 0 occupations for $\alpha = 1, 2, \ldots, M/2 - 1$ and have either 0 or N occupations for flavor $\alpha = M/2$. These conditions completely fix the possible lowest-weight states:

$$|0\rangle, \quad |0^\zeta\rangle \equiv c_{1,M/2}^\dagger c_{2,M/2}^\dagger \cdots c_{N,M/2}^\dagger |0\rangle, \qquad (32)$$

where $|0^\zeta\rangle$ can be thought as the multiflavor generalization of the ζ vacuum. They are both manifestly SO(N) invariant. The state $|0\rangle$ is annihilated by $\eta_{\alpha\beta}$, $\zeta_{\alpha\beta}$, and $\zeta_{\alpha\beta}^\dagger$. The state $|0^\zeta\rangle$ is annihilated by all $\eta_{\alpha\beta}$ and $\zeta_{\alpha\beta}$, and $\zeta_{\alpha\beta}^\dagger$ with $\beta < M/2$, because they contain at least one annihilation operator of

flavor $1, 2, \ldots, M/2 - 1$. It is also annihilated by $\eta^\dagger_{\alpha, M/2}$ since it is fully filled at flavor $M/2$.

Denote the irreducible representation containing $|0\rangle$ by $\mathcal{H}_\eta$, which corresponds to the highest-weight vector $\lambda_\eta = (\frac{N}{2}, \frac{N}{2}, \ldots, (-1)^{M/2} \frac{N}{2})$, and denote the irreducible representation containing $|0^\zeta\rangle$ by $\mathcal{H}_\zeta$, which corresponds to the highest-weight vector $\lambda_\zeta = (\frac{N}{2}, \frac{N}{2}, \ldots, (-1)^{M/2+1} \frac{N}{2})$. Then the singlet subspace $\mathbb{S}$ is a direct sum of $\mathcal{H}_\eta \oplus \mathcal{H}_\zeta$, i.e., $n_+ = n_- = 1$ in Eq. (31). States in $\mathcal{H}_\eta$ are obtained by acting with all

$$\eta^\dagger_{\alpha\beta} = \sum_j c^\dagger_{j\alpha} c^\dagger_{j\beta} \qquad (33)$$

repeatedly on the empty vacuum $|0\rangle$, and hence are generalizations of η states in the Hubbard model. Similarly, $\mathcal{H}_\zeta$ is built with $\zeta^\dagger_{\beta, M/2} = \sum_j c^\dagger_{j\beta} c_{j, M/2}$ ($1 \leqslant \beta \leqslant M/2 - 1$) and $\eta^\dagger_{\alpha\beta}$ ($1 \leqslant \alpha < \beta \leqslant M/2 - 1$) on $|0^\zeta\rangle$, which generalizes ζ states in the Hubbard model.

The two representations $\mathcal{H}_\eta$ and $\mathcal{H}_\zeta$ are always distinguished by a reflection operator in $O(N)$, which can be realized by $e^{i\pi n_j}$ (the site j can be chosen arbitrarily). $\mathcal{H}_\eta$ has parity $+1$ under $e^{i\pi n_j}$ and hence is $O(N)$ invariant. $\mathcal{H}_\zeta$, on the other hand, has parity -1 under $e^{i\pi n_j}$ and hence is only $SO(N)$ invariant. The fully occupied state, which is apparently a highest-weight state, has parity $(-1)^{M/2}$ under the reflection $e^{i\pi n_j}$. So it belongs to $\mathcal{H}_\eta$ when $M/2$ is even and $\mathcal{H}_\zeta$ when $M/2$ is odd. This also explains why the highest weight vectors of $\mathcal{H}_\eta$ and $\mathcal{H}_\zeta$ depend on the parity of $M/2$. When N is odd, $\mathcal{H}_\eta$ and $\mathcal{H}_\zeta$ can also be distinguished by the fermionic parity (18). In this case, $\mathcal{H}_\eta$ has fermionic parity $+1$ and $\mathcal{H}_\zeta$ has fermionic parity -1.

Altogether, there are $\dim \mathcal{H}_\eta$ linearly independent $O(N)$ singlets and $2 \dim \mathcal{H}_\eta$ linearly independent $SO(N)$ singlets. The explicit expression of $\dim \mathcal{H}_\eta$ can be derived using Weyl dimension formula (A9). Some small M examples are as follows:

$$M = 4 : N + 1$$
$$M = 6 : \binom{N+3}{3}$$
$$M = 8 : \frac{N+3}{3} \binom{N+5}{5}. \qquad (34)$$

The general formula for the dimension of the singlet states is given by

$$D(N, M) = \frac{\prod_{i=1}^{M+1-4i>0} \binom{N+M-1-2i}{M+1-4i}}{\prod_{i=1}^{M+1-4i>0} \binom{M-1-2i}{M+1-4i}}. \qquad (35)$$

We note that, for a fixed even M, the number of singlet states grows at large N as $\dim \mathcal{H}_\eta \sim N^{\frac{M(M-2)}{8}}$. If we fix N and consider large M, then we get $\dim \mathcal{H}_\eta \sim e^{0.22NM}$.

B. Energy spectrum and degeneracy

For the full Hamiltonian $H = T_M + H_\mu + V_M + \widetilde{H}_{\rm int}$ given by Eq. (24) [same when $\widetilde{H}_{\rm int}$ is replaced by H_{OT} (26)], its spectrum in $\mathbb{S} = \mathcal{H}_\eta \oplus \mathcal{H}_\zeta$ is determined by H_μ and V_M. The spectrum of V_M is particularly simple. Noticing that it is even under the reflection $e^{i\pi n_j}$, we have $V_M \mathcal{H}_\eta \subset \mathcal{H}_\eta$ and $V_M \mathcal{H}_\zeta \subset \mathcal{H}_\zeta$. Since $\mathcal{H}_\eta$ and $\mathcal{H}_\zeta$ are irreducible representations of $SO(M)$, we can use Schur's lemma to argue that the $SO(M)$-invariant operator V_M becomes a constant when restricted to either $\mathcal{H}_\eta$ or $\mathcal{H}_\zeta$. Using $V_M |0\rangle = 0$ and $V_M |0^\zeta\rangle = -2^{1-\frac{M}{2}} NU |0^\zeta\rangle$, we conclude

$$V_M|_{\mathcal{H}_\eta} = 0, \quad V_M|_{\mathcal{H}_\zeta} = -2^{1-\frac{M}{2}} NU. \qquad (36)$$

The spectrum of the chemical potential term H_μ restricted to $\mathbb{S}$ is encoded in the partition function $\mathcal{Z}(\beta) \equiv \mathrm{tr}_{\mathbb{S}}\, e^{-\beta \sum_\alpha \mu_\alpha h_\alpha}$, which group theoretically is equal to the sum of two $SO(M)$ characters,

$$\mathcal{Z}(\beta) = \chi^{\mathrm{SO}(M)}_{\lambda_\eta}(\boldsymbol{x}) + \chi^{\mathrm{SO}(M)}_{\lambda_\zeta}(\boldsymbol{x}), \qquad (37)$$

where $x_\alpha \equiv e^{-\beta \mu_\alpha}$. Each character can be computed using Weyl character formula (A8). These Weyl characters admit the following expansions:

$$\chi^{\mathrm{SO}(M)}_{\lambda_\eta}(\boldsymbol{x}) = \sum_{\boldsymbol{p}} D^\eta_{\boldsymbol{p}} \prod_\alpha x_\alpha^{p_\alpha}$$
$$\chi^{\mathrm{SO}(M)}_{\lambda_\zeta}(\boldsymbol{x}) = \sum_{\boldsymbol{p}} D^\zeta_{\boldsymbol{p}} \prod_\alpha x_\alpha^{p_\alpha}, \qquad (38)$$

where $\{p_\alpha\}$ take values in all integers when N is even and all half integers when N is odd. The coefficients $D^\eta_{\boldsymbol{p}}$ ($D^\zeta_{\boldsymbol{p}}$) are non-negative integers, and they vanish for all but a finite number of vectors $\boldsymbol{p}$. Because of the identification $x_\alpha = e^{-\beta \mu_\alpha}$, the characters implies that there are $D^\eta_{\boldsymbol{p}}$ ($D^\zeta_{\boldsymbol{p}}$) linearly independent states in $\mathcal{H}_\eta$ ($\mathcal{H}_\zeta$) that diagonalize all $\{h_\alpha\}$ simultaneously with eigenvalues $\{p_\alpha\}$. Altogether, the eigenenergies of the full Hamiltonian restricted to the scar subspace can be summarized as

$$\mathcal{H}_\eta : \left\{ \sum_\alpha -\mu_\alpha \left(p_\alpha + \frac{N}{2}\right), \text{ for all } \boldsymbol{p} \text{ satisfying } D^\eta_{\boldsymbol{p}} > 0 \right\}$$

$$\mathcal{H}_\zeta : \left\{ \sum_\alpha -\mu_\alpha \left(p_\alpha + \frac{N}{2}\right) - \frac{NU}{2^{\frac{M}{2}-1}}, \text{ for all } \boldsymbol{p} \text{ satisfying } D^\zeta_{\boldsymbol{p}} > 0 \right\}. \qquad (39)$$

For finite given N and M the expansion (38) can be performed analytically or using analytical math software

and the positive $D_{\boldsymbol{p}}$ can be read off from it. Therefore the spectrum in the scar subspace is known exactly analytically

for the systems that we study numerically in Secs. VI and VIII.

For generic chemical potentials μ_α and interaction strength U, the energy spacing does not have a common divisor. So we will not observe revivals starting from a generic state in $\mathbb{S}$. However, because $\{p_\alpha\}$ are integers or half-integers, revivals are possible with special choices of μ_α,

$$\frac{\mu_\alpha}{\mu_\beta} \in \mathbb{Q}, \qquad \frac{\mu_\alpha}{2NU} \in \mathbb{Q}, \tag{40}$$

where the second condition can be removed if we only consider scars in $\mathcal{H}_\eta$ or $\mathcal{H}_\zeta$.

When $M = 4$ or 6, $D_{\boldsymbol{p}}^\eta$ and $D_{\boldsymbol{p}}^\zeta$ are either 0 or 1, which means that H_μ does not have any degenerate energy level within $\mathcal{H}_\eta$ or $\mathcal{H}_\zeta$. On the other hand, double degeneracy happens between $\mathcal{H}_\eta$ and $\mathcal{H}_\zeta$ when N is even. This does not happen for odd N because $\mathcal{H}_\eta$ and $\mathcal{H}_\zeta$ are distinguished by fermionic parity when N is odd. For instance, when $M = 6$ and $N = 4$, H_μ has 19 doubly degenerate energy levels. Such degeneracies are broken by V_M. When $M \geqslant 8$, $D_{\boldsymbol{p}}^\eta$ and $D_{\boldsymbol{p}}^\zeta$ can be larger than 1. It corresponds to degeneracies within $\mathcal{H}_\eta$ or $\mathcal{H}_\zeta$ and hence cannot be removed by V_M. For example, the three states $\eta_{12}^\dagger \eta_{34}^\dagger |0\rangle$, $\eta_{13}^\dagger \eta_{24}^\dagger |0\rangle$, and $\eta_{14}^\dagger \eta_{23}^\dagger |0\rangle$ have the same quantum numbers with respect to the Cartan generators and hence have the same energy. Indeed, when $M = 8$ and $N = 4$, the case studied numerically in Sec. VI B, $\mathcal{H}_\eta$ contains 32 triply degenerate energy levels, and one energy level with degeneracy 6. The same degeneracies are present in $\mathcal{H}_\zeta$, in agreement with numerical findings.

We conjecture that the remaining degeneracies we observe for $M > 6$ are "unbreakable," i.e., they cannot be removed by any *local* perturbations that preserve the decoupling of the scars. If we allow nonlocal terms, then using the second term in (44) we can easily break the degeneracies. For instance, we can consider

$$H_2^{\mathrm{nl}} = \sum_{A,B=1}^{M} r_{AB} (J^{AB})^2, \tag{41}$$

where r_{AB} are a set of real random numbers or

$$H_m^{\mathrm{nl}} = \sum_{A,B,C,D=1}^{M} r_{ABCD} (J^{AB} J^{CD}), \tag{42}$$

where r_{ABCD} are real random numbers and the sum over A, B, C, D only includes combinations where either all the four indexes are different or $A, B = C, D$ (to ensure each term is Hermitian).

A proof of the degeneracies for local Hamiltonians may proceed along the following lines. The Hamiltonian that supports the $SO(N)$ singlet states as eigenstates must have the following form [22]:

$$H = H_s + \sum_{i<j,A} O_{ij} \psi_i^A \psi_j^A, \tag{43}$$

where H_s is a singlet operator and $\sum_A \psi_i^A \psi_j^A$ is a generator of $SO(N)$. The idea is to consider all possible terms that can enter into H_s and to show that they can be separated into three groups: (a) those that preserve the degeneracies within the scar subspace and are local; (b) those that preserve the

degeneracies within the scar subspace and are nonlocal, but their nonlocality can be "fixed" by adding a suitable OT term; and (c) those that may break the scar degeneracies but are then necessarily nonlocal and cannot be made local by means of adding an OT term. Therefore the locality of the Hamiltonian H is considered as a whole while its individual summands may be nonlocal. The locality in our definition means in particular that there exists some number K such that for any term in H any two Majorana operators in it are not too far $\psi_i^A, \psi_j^B \ |i - j| < K$.

The most general form of H_s is

$$H_s = \mu_{AB} \sum_i \psi_i^A \psi_i^B + \nu_{ABCD} \sum_{i,j} \psi_i^A \psi_i^B \psi_j^C \psi_j^D + \cdots$$
$$+ \lambda \sum_{i,\dots,j} \epsilon_{A_1 A_2 \dots A_{M-1} A_M} \psi_i^{A_1} \psi_i^{A_2} \dots \psi_j^{A_{M-1}} \psi_j^{A_M}, \tag{44}$$

where we group terms by the (even) number of contributing Majorana operators and where ν_{ABCD} is an arbitrary tensor and $\epsilon_{A_1 A_2 \dots A_{M-1} A_M} \psi_i^{A_1} \psi_i^{A_2} \dots \psi_j^{A_{M-1}} \psi_j^{A_M}$ is the fully antisymmetric tensor. We can consider these terms separately.

The first term, the chemical potential, is obviously local, since only the fermions on the same site interact. The second and last term in (44) are obviously nonlocal. For the last term in (44), however, we can add such a combination of OT terms that reduces it to the local V_M defined in (19). While for the second term through exhaustive search (considering the two-site, four-Majorana operators with $M = 6$), we found that there is no OT term capable of removing its nonlocality for arbitrary ν_{ABCD}. At present, we do not have the complete proof for other terms, which contain six or more Majorana operators, but we conjecture that there exists no such OT term that could make these intermediate terms in H_s local.

In summary, all the terms in H_s but first and last are eliminated by the locality requirement and we see that any local H_s is a sum of an element of Lie algebra $\mathfrak{so}(M)$ (chemical potential term) and generalized Hubbard interaction V_M (only shifts scar energy by a constant). This leads us to conjecture that the scar subspace spectrum is fully determined by this first chemical potential term as long as the Hamiltonian is required to be local. Its spectrum can be computed using the Weyl character formula [64] and therefore contains certain ("unbreakable") degeneracies.

C. Product scar states

Product states are very special because their entanglement entropy vanishes. In $\mathbb{S}$, product states are either empty or fully filled for each of the $M/2$ flavors. Hence there are $2^{M/2}$ such states. To describe their wave functions, we define the following N-fermion operators:

$$\mathcal{A}_\alpha^\dagger \equiv c_{1\alpha}^\dagger c_{2\alpha}^\dagger \cdots c_{N\alpha}^\dagger, \qquad \alpha = 1, 2, \dots, M/2. \tag{45}$$

Then the $2^{M/2}$ product states can be expressed as

$$|\alpha_1, \dots, \alpha_\kappa\rangle = \mathcal{A}_{\alpha_1}^\dagger \cdots \mathcal{A}_{\alpha_\kappa}^\dagger |0\rangle, \tag{46}$$

where $1 \leqslant \alpha_1 < \alpha_2 < \cdots < \alpha_\kappa \leqslant M/2$. In particular, $\kappa = 0$ corresponds to the empty vacuum $|0\rangle$, and $\kappa = M/2$ corresponds to the fully occupied state. Since $\mathcal{A}_\alpha^\dagger$ has odd parity under the reflection $e^{i\pi n_j}$, the product state $|\alpha_1, \dots, \alpha_\kappa\rangle$

belongs to $\mathcal{H}_\eta$ when κ is even and $\mathcal{H}_\zeta$ when κ is odd. For the full Hamiltonian H, cf. Eq. (24), $|\alpha_1, \ldots, \alpha_\kappa\rangle$ is an eigenstate with energy

$$E_{\alpha_1 \cdots \alpha_\kappa} = -N \sum_{m=1}^{\kappa} \mu_{\alpha_m} + \frac{(-1)^\kappa - 1}{2^{\frac{M}{2}}} NU. \quad (47)$$

In the case of $M = 4$, the product states in $\mathbb{S}$ are

$$\kappa = 0 : \ |0\rangle, \quad \kappa = 2 : \ |1, 2\rangle = \mathcal{A}_1^\dagger \mathcal{A}_2^\dagger |0\rangle$$
$$\kappa = 1 : \ |1\rangle = \mathcal{A}_1^\dagger |0\rangle, \quad |2\rangle = \mathcal{A}_2^\dagger |0\rangle, \quad (48)$$

where the $\kappa = 0$ and $\kappa = 2$ states are η states $|0^\eta\rangle$ and $|N^\eta\rangle$ [cf. Eq. (9)], and the two $\kappa = 1$ states are ζ states $|0^\zeta\rangle$ and $|N^\zeta\rangle$ [cf. Eq. (10)], which have total spin $\pm\frac{N}{2}$.

D. The $M = 6$ case

When $M = 6$, the O(N)-invariant subspace $\mathcal{H}_\eta$ has dimension $\binom{N+3}{3}$. Consider states in $\mathcal{H}_\eta$ of the form $(\eta_{12}^\dagger)^{k_{12}}(\eta_{13}^\dagger)^{k_{13}}(\eta_{23}^\dagger)^{k_{23}}|0\rangle$. First, by a direct computation, we find that $(\eta_{12}^\dagger)^{k_{12}}(\eta_{13}^\dagger)^{k_{13}}(\eta_{23}^\dagger)^{k_{23}}|0\rangle$ has the norm $\frac{N!k_{12}!k_{13}!k_{23}!}{(N-k_{12}-k_{13}-k_{23})!}$ and hence is nonvanishing when $k_T \equiv k_{12} + k_{13} + k_{23} \leqslant N$. Next, these states are linearly independent, because $\{k_{12}, k_{13}, k_{23}\}$ uniquely fixes the fermion numbers of the three flavors, namely $k_{12} + k_{13}$ particles of flavor 1, $k_{12} + k_{23}$ particles of flavor 2 and $k_{13} + k_{23}$ particles of flavor 3. Finally, counting nonnegative integer solutions of the inequality $k_{12} + k_{13} + k_{23} \leqslant N$ precisely reproduces $\binom{N+3}{3}$. Therefore, an orthonormal basis of $\mathcal{H}_\eta$ that diagonalizes the three Cartan generators $\{h_1, h_2, h_3\}$ simultaneously is

$$|k_{12}, k_{13}, k_{23}\rangle = C_{\boldsymbol{k}}(N) \prod_{1 \leqslant \alpha < \beta \leqslant 3} (\eta_{\alpha\beta}^\dagger)^{k_{\alpha\beta}} |0\rangle, \quad k_T \leqslant N, \quad (49)$$

where the normalization factor $C_{\boldsymbol{k}}(N)$ is given by

$$C_{\boldsymbol{k}}(N) = \sqrt{\frac{(N - k_T)!}{N! k_{12}! k_{13}! k_{23}!}}. \quad (50)$$

These states (49) are also constructed in Ref. [43] as energy eigenvectors of the SU(3) Hubbard model. The eigenenergy of $|k_{12}, k_{13}, k_{23}\rangle$ with respect to our full Hamiltonian H is

$$E_\eta(k_{12}, k_{13}, k_{23}) = -\sum_{i<j} k_{ij}(\mu_i + \mu_j). \quad (51)$$

For the SO(N)-invariant subspace $\mathcal{H}_\zeta$, we can construct an orthonormal basis similarly

$$|k_{12}, k_{13}, k_{23}\rangle^\zeta = C_{\boldsymbol{k}}(N)(\eta_{12}^\dagger)^{k_{12}}(\zeta_{13}^\dagger)^{k_{13}}(\zeta_{23}^\dagger)^{k_{23}}|0^\zeta\rangle, \quad k_T \leqslant N. \quad (52)$$

They are eigenstates of the Hamiltonian (24) with energy

$$E_\zeta(k_{12}, k_{13}, k_{23}) = -\sum_{i<j} k_{ij}(\widetilde{\mu}_i + \widetilde{\mu}_j) + N\widetilde{\mu}_3 - \frac{NU}{2^{\frac{M}{2}-1}}, \quad (53)$$

where $\widetilde{\mu}_{1,2} = \mu_{1,2}, \widetilde{\mu}_3 = -\mu_3$.

With the explicit wave functions of all the SO(N) singlets in the $M = 6$ case, we can calculate their entanglement entropy analytically (more details can be found in the Appendix C). We will focus on $\mathcal{H}_\eta$ but the same method works for $\mathcal{H}_\zeta$. A similar calculation was performed for the η states in usual Hubbard model [10], and for a special class of η states in multicomponent Hubbard model in Ref. [43]. In the thermodynamic limit we find that the entropy $S_{N_1}(\boldsymbol{k})$ scales as the *logarithm* of N_1, the number of sites in the subsystem Σ_1,

$$S_{N_1}(k_{12}, k_{13}, k_{23}) \sim \frac{3}{2} \log(N_1), \quad (54)$$

where $k = k_{12} + k_{23} + k_{13}$. This result does not depend on the dimensionality of the original system. The coefficient $\frac{3}{2}$ for the logarithmic behavior agrees with a calculation in Ref. [43]. Let us note that the coefficient $\frac{3}{2}$ applies only to the most typical η states where k_{12}, k_{13}, and k_{23} are all large. If only two of them are large, then the coefficient of $\log(N_1)$ is reduced to 1; if only one of them is large, then it is reduced to $1/2$.

E. The structure of singlets for $M \geqslant 8$

When $M = 8$, there are six different $\eta_{\alpha\beta}^\dagger$. In order to construct explicit wave functions of $\mathcal{H}_\eta$, we consider the following set of states, which generalizes the $M = 6$ case:

$$V_\eta^{\mathrm{I}} \equiv \mathrm{Span}\left\{ \prod_{\alpha<\beta} (\eta_{\alpha\beta}^\dagger)^{k_{\alpha\beta}}|0\rangle, \quad \sum_{\alpha<\beta} k_{\alpha\beta} \leqslant N \right\}. \quad (55)$$

A simple counting yields $\dim V_\eta^{\mathrm{I}} = \binom{N+6}{6}$, which is smaller than $\frac{N+3}{3}\binom{N+5}{5}$, i.e., the dimension of $\mathcal{H}_\eta$ when $M = 8$. It means that V_η^{I} is only a subset of $\mathcal{H}_\eta$. For example, the fully filled state $|\bar{0}\rangle = \prod_\alpha^4 \prod_{j=1}^N c_{j\alpha}^\dagger |0\rangle$ does not belong to V_η^{I}. Noticing that $|\bar{0}\rangle$ is actually the highest-weight state of $\mathcal{H}_\eta$, we build on it another set of states

$$V_\eta^{\mathrm{II}} \equiv \mathrm{Span}\left\{ \prod_{\alpha<\beta} (\eta_{\alpha\beta})^{\ell_{\alpha\beta}}|\bar{0}\rangle, \quad \sum_{\alpha<\beta} \ell_{\alpha\beta} < N \right\}, \quad (56)$$

which has dimension $\binom{N+5}{6}$. Since states in V_η^{I} have total fermion number $Q \leqslant 2N$ and states in V_η^{II} have total fermion number $Q > 2N$, the two sets V_η^{I} and V_η^{II} have no intersection. Adding up their dimensions gives exactly the dimension of $\mathcal{H}_\eta$. Therefore an orthonormal basis of $\mathcal{H}_\eta$ is

$$\prod_{\alpha<\beta} (\eta_{\alpha\beta}^\dagger)^{k_{\alpha\beta}}|0\rangle, \quad \prod_{\alpha<\beta} (\eta_{\alpha\beta})^{\ell_{\alpha\beta}}|\bar{0}\rangle, \quad (57)$$

where $k_{\alpha\beta}$ and $\ell_{\alpha\beta}$ satisfy $\sum_{\alpha<\beta} k_{\alpha\beta} \leqslant N$, $\sum_{\alpha<\beta} \ell_{\alpha\beta} < N$.

Similarly, one can show that $\mathcal{H}_\zeta$ is an orthonormal direct sum of V_ζ^{I} which is spanned by

$$\prod_{1 \leqslant \alpha < \beta \leqslant 3} (\eta_{\alpha\beta}^\dagger)^{k_{\alpha\beta}} \prod_{1 \leqslant \gamma \leqslant 3} (\zeta_{\gamma 4}^\dagger)^{k_{\gamma 4}} |0^\zeta\rangle, \quad \sum_{\alpha<\beta} k_{\alpha\beta} \leqslant N, \quad (58)$$

and V_ζ^{II} which is spanned by

$$\prod_{1 \leqslant \alpha < \beta \leqslant 3} (\eta_{\alpha\beta})^{\ell_{\alpha\beta}} \prod_{1 \leqslant \gamma \leqslant 3} (\zeta_{\gamma 4})^{\ell_{\gamma 4}} |\bar{0}^\zeta\rangle, \quad \sum_{\alpha<\beta} \ell_{\alpha\beta} < N, \quad (59)$$

where $|\bar{0}^\zeta\rangle = \prod_{\alpha=1}^3 \prod_{j=1}^N c_{j\alpha}^\dagger |0\rangle$ is the highest-weight state of $\mathcal{H}_\zeta$. The basis of V_η^{I}, V_η^{II}, V_ζ^{I}, and V_ζ^{II} are eigenstates of the

Hamiltonian H, and their corresponding eigenenergies can be easily derived by reading off the fermion number of each flavor. For example, the energy of $\prod_{\alpha<\beta}(\eta_{\alpha\beta}^{\dagger})^{k_{\alpha\beta}}|0\rangle$ is

$$E_{\eta}(\boldsymbol{k}) = -\sum_{\alpha<\beta} k_{\alpha\beta}(\mu_{\alpha}+\mu_{\beta}). \tag{60}$$

We will compute their entanglement entropy numerically in the next section.

For $M \geqslant 10$, it becomes very hard to write down explicit wave functions of all SO(N) singlets.

In Ref. [43], some special states belonging to $\mathcal{H}_{\eta}$ are considered, namely $(\eta_{12}^{\dagger})^{k_2}\cdots(\eta_{1,M/2}^{\dagger})^{k_{M/2}}|0\rangle$ with $k_2+\cdots+k_{M/2}\leqslant N$. They are eigenstates of the generalized Hubbard potential (27) and their entanglement entropy can be evaluated analytically. In the thermodynamic limit, the entanglement entropy is found to scale as $S_{\Sigma_1}\sim\frac{M-2}{4}\log N_1$ [43]. When $M=6$, this expression gives $S_{\Sigma_1}\sim\log N_1$, different from what we found in Eq. (C6). The difference is because $S_{\Sigma_1}\sim\log N_1$ corresponds to the entanglement entropy of η states $(\eta_{12}^{\dagger})^{k_{12}}(\eta_{13}^{\dagger})^{k_{13}}|0\rangle$, which do not involve η_{23}. These special η states are not captured by the analysis in Sec. IV D, since the thermodynamic limit there requires all three $\frac{k_{ij}}{N}$ to be finite as $N\to\infty$.

F. Off-diagonal long-range order

By construction, the singlet states have long-range correlations, and we can confirm this by studying the spatial dependence of the following operators:

$$O_{ij}^{AB}(s) = \langle s|\psi_i^A\psi_i^B\psi_j^B\psi_j^A|s\rangle. \tag{61}$$

It is easy to check that if $i\neq j$, then this operator is real and does not depend on the indices i and j. Indeed, let us consider a rotation Q_{ik} that acts in the (i,k) plane and leaves the rest of the vectors untouched. Then it is easy to check that

$$O_{ij}^{AB}(s) = \langle s|\psi_i^A\psi_i^B\psi_j^B\psi_j^A|s\rangle = \langle s|Q_{ik}^{-1}\psi_i^A\psi_i^B\psi_j^B\psi_j^A Q_{ik}|s\rangle$$
$$= \langle s|\psi_k^A\psi_k^B\psi_j^B\psi_j^A|s\rangle = O_{kj}^{AB}(s) = O^{AB}(s), \tag{62}$$

the value of this operator does not depend on the spatial indexes. Therefore the associated correlations do not decay and remain finite and constant at arbitrary distances. The expectation value (61) depends on the choice of flavors AB and the singlet state $|s\rangle\in\mathbb{S}$. But if we sum over A and B we would get a simpler operator,

$$O(s) = \sum_{A\neq B} O^{AB}(s) = \sum_{A\neq B}\langle s|\psi_i^A\psi_i^B\psi_j^B\psi_j^A|s\rangle$$
$$= -\sum_{A\neq B}\langle s|\psi_i^A\psi_j^A\psi_j^B\psi_i^B|s\rangle, \tag{63}$$

where we have used anticommutation relations. After that we can get

$$O(s) = -\sum_{A,B}\langle s|\psi_i^A\psi_j^A\psi_j^B\psi_i^B|s\rangle + \sum_{A=B}\langle s|\psi_i^A\psi_j^A\psi_j^B\psi_i^B|s\rangle$$
$$= \sum_{A=B}\langle s|\psi_i^A\psi_j^A\psi_j^B\psi_i^B|s\rangle = \frac{M}{4}, \tag{64}$$

where we have used the fact that $|s\rangle$ is annihilated by the action of hopping $T_{ij} = \sum_A \psi_i^A\psi_j^A$ and the last equality follows from the anticommutation relations (11).

Another "sum rule" arises if we average O_{ij}^{AB} over all the singlet states,

$$\widetilde{O}^{AB} = \frac{1}{\dim\mathbb{S}}\sum_{|s\rangle\in\mathbb{S}} O_{ij}^{AB}(s), \tag{65}$$

which amounts to computing the trace of $\psi_i^A\psi_i^B\psi_j^B\psi_j^A$ over the scar subspace. When $i\neq j$, its value is independent of the choice of i,j. For $A\neq B$, we have

$$\sum_{i,j}\frac{\mathrm{tr}_{\mathbb{S}}(\psi_i^A\psi_i^B\psi_j^B\psi_j^A)}{\dim\mathbb{S}} = N(N-1)\widetilde{O}^{AB} + \frac{N}{4}, \tag{66}$$

where $\dim\mathbb{S} = 2\dim\mathcal{H}_{\eta}$ is the dimension of scar sector [see Eq. (34) for explicit expressions of $\dim\mathcal{H}_{\eta}$ when M is small]. On the left-hand side of Eq. (66), the double sum over i,j yields $J^{AB}J^{BA}$. Noticing that $\mathrm{tr}_{\mathbb{S}}(J^{AB}J^{BA})$ is actually independent of A,B, we can replace it by $\sum_{A<B}\mathrm{tr}_{\mathbb{S}}(J^{AB}J^{BA})/[\frac{1}{2}M(M-1)]$. The sum over A,B leads to the Casimir of SO(M) and the latter is a constant in the scar subspace with its value given by $\frac{MN}{8}(M+N-2)$. Altogether, we obtain the value of $\widetilde{O}^{AB}$:

$$\widetilde{O}^{AB} = \frac{1}{4(M-1)}, \tag{67}$$

which implies that $O^{AB}(s)$ is nonvanishing for at least one $|s\rangle$.

V. A BOUND ON THE ENTANGLEMENT ENTROPY OF SINGLET STATES

An upper bound on the entanglement entropy of singlet states can be obtained without knowing the explicit wave functions. We will derive the bound for η states and it will be easy to see that the same bound also holds for ζ states. As noted earlier, we may divide the full lattice into two disjoint sublattices $\Sigma_1\cup\Sigma_2$, with N_a sites in Σ_a. Let N_1 be much smaller than $N_2 = N-N_1$, but still a large number in the thermodynamic limit. On each sublattice Σ_a, we can construct its own η operators $\eta_{\alpha\beta}^{a\dagger}$ that create O(N_a) singlets on the empty vacuum $|0\rangle_a$. We use $\mathcal{H}_{\eta}^a$ to denote the sub-Hilbert space spanned by all O(N_a) singlets on Σ_a. The dimension of $\mathcal{H}_{\eta}^a$ is given by $D(N_a,M)$, cf. Eq. (35). Recall that an O(N)-invariant state is constructed by acting with $\eta_{\alpha\beta}^{\dagger}$ on $|0\rangle$. Because $\eta_{\alpha\beta}^{\dagger} = \sum_{a=1}^2 \eta_{\alpha\beta}^{a\dagger}$ and $|0\rangle = |0\rangle_1\otimes|0\rangle_2$, the O($N$)-invariant state should also belong to $\mathcal{H}_{\eta}^1\otimes\mathcal{H}_{\eta}^2$. Applying the Schmidt decomposition to this tensor product yields that for any $|s\rangle\in\mathcal{H}_{\eta}$, we have

$$|s\rangle = \sum_{n=1}^{D(N_1,M)}\Lambda_n|s_n^1\rangle\otimes|s_n^2\rangle, \quad \sum_{n=1}^{D(N_1,M)}\Lambda_n^2 = 1, \tag{68}$$

where $|s_n^a\rangle$ are orthonormal states in $\mathcal{H}_{\eta}^a$ and are most importantly O(N_a) invariant. We observe that the number of the nonzero terms in the decomposition (68) is significantly reduced compared to the full dimension of the subsystem Σ_1 ($2^{N_1 M/2}$). Then it is clear that the entanglement entropy of $|s\rangle$

in the subsystem Σ_1 is bounded by $\log D(N_1, M)$ from above

$$S_{\text{EE}} \leqslant \log D(N_1, M). \tag{69}$$

For the $O(N)$ singlets we can use the formula (35) and its asymptotic expansion in the thermodynamic limit $D(N_1, M) \sim N_1^{\frac{M(M-2)}{8}}$, which leads to the bound

$$S_{\text{EE}} \lesssim \frac{M(M-2)}{8} \log N_1. \tag{70}$$

Based on our explicit calculations, such as (C6), we conjecture that the maximum entropy of the scar states in the thermodynamic limit instead grows as

$$S_{\text{EE}} \to \frac{M(M-2)}{16} \log N_1, \tag{71}$$

which suggests that the bound (69) is far from being saturated.

We can generalize the argument above to other systems with an action ρ of some group G on the total Hilbert space $\mathcal{H}$. We assume that G has two subgroups, G_1 and G_2, satisfying the following conditions: (i) $G_1 \times G_2 \subset G$, (ii) $G_1 \cap G_2 = \{e\}$, and (iii) the restriction of ρ to each G_a gives a representation of G_a on the Hilbert space $\mathcal{H}^a$ of the subsystem supported on Σ_a. In each $\mathcal{H}^a$, there is a subspace $\mathcal{H}_0^a$ consisting of G_a singlets. We denote the dimension of $\mathcal{H}_0^a$ by $D(N_a)$ and assume that $D(N_1) \leqslant D(N_2)$. The projection of $\mathcal{H}^a$ to $\mathcal{H}_0^a$ can be implemented by the projector $P_a \equiv \int_{G_a} dg_a \, \rho(g_a)$, where dg_a is the normalized Haar measure on G_a. Now let us consider a generic G-singlet $|s\rangle \in \mathcal{H}$. Because of the tensor product structure $\mathcal{H} = \mathcal{H}^1 \otimes \mathcal{H}^2$, $|s\rangle$ can be expressed schematically as $|s\rangle = \sum_\kappa |\psi_\kappa^1\rangle \otimes |\psi_\kappa^2\rangle$, where $|\psi_\kappa^a\rangle \in \mathcal{H}^a$. Applying the projectors P_1 and P_2 to $|s\rangle$ yields $P_1 P_2 |s\rangle = \sum_\kappa P_1 |\psi_\kappa^1\rangle \otimes P_2 |\psi_\kappa^2\rangle$. The left-hand side is just equal to $|s\rangle$, while on the right-hand side $P_{1,2}$ projects onto the singlet subspace $\mathcal{H}_0^{1,2}$. Therefore $|s\rangle$ belongs to $\mathcal{H}_0^1 \otimes \mathcal{H}_0^2$. Using the Schmidt decomposition for this tensor product, we get a generalization of Eq. (68),

$$|s\rangle = \sum_{n=1}^{D(N_1)} \Lambda_n |s_n^1\rangle \otimes |s_n^2\rangle, \quad \sum_{n=1}^{D(N_1)} \Lambda_n^2 = 1, \tag{72}$$

where $|s_n^a\rangle$ are orthonormal states and singlets in $\mathcal{H}^a$. In other words, cutting a singlet state we always get two subsystem states that are also singlets and this condition significantly reduces the number of nonzero singular values contributing to the sum. This means that the entanglement entropy of any G-invariant state over Σ_1 is bounded by

$$S_{\text{EE}}^G \leqslant \log(D(N_1)). \tag{73}$$

The bound (73) actually allows us to conclude that the G-invariant many-body scars that appear in models built according to the general $H_0 + OT$ prescription [22] always have the entanglement entropy that is significantly lower than that of generic excited states. From analogous bound for the typical excited state we can conclude that $S_{\text{EE}} \leqslant \log \dim \mathcal{H}^1 \sim N_1$. On the other hand, the bound on the entropy of the group-invariant many-body scars is (73). If we assume that these bounds are parametrically correct and that $D(N_1) \ll \dim \mathcal{H}^1$, then the entanglement entropy of singlet states is parametrically smaller than that of the generic states.

Most of the many-body scars reported in the literature are characterized by anomalously low entanglement entropy. We conjecture that this can be explained by the same mechanism. The scars have a decomposition similar to (72) and the dimension of the subsystem states compatible with the scar states structure is significantly smaller than the full subsystem dimension which leads [see Eq. (73)] to lower entanglement. A special case of this situation is when cutting a scar necessarily gives scar states in the subsystems which is true for group-invariant scars [22].

Finally, we note that our entanglement scaling for the η states in the single-band case is in agreement with the results obtained by the method [65] where local correlation matrix is analyzed numerically to deduce a bound on the entanglement entropy of a quantum state. It has also been noticed [42] that the same method [65] is useful for bounding the entanglement of the many-body scars built using the Shiraishi-Mori approach [3].

VI. NUMERICAL RESULTS

To test our analytical predictions numerically we implement the Hamiltonian (24) that was argued in Sec. III A to support singlet many-body scars

$$H = -\sum_{\alpha=1}^{M/2} \mu_\alpha \sum_j n_{j\alpha} + U \sum_j i^{M/2} \psi_j^1 \psi_j^2 \cdots \psi_j^M$$
$$+ it \sum_{\langle j,k \rangle} T_{jk} + p H_{\text{SB}} - \frac{N}{2^{\frac{M}{2}}} U, \tag{74}$$

where the auxiliary symmetry-breaking term H_{SB} is given by either a three-body [$H_{\text{SB}} = \tilde{H}_{\text{int}}$ from Eq. (23)] or two-body [$H_{\text{SB}} = H_{\text{OT}}$ from Eq. (26)] interactions. The hopping strength is set to $t = 1$.

The values of chemical potentials μ_α and parameters p and U will be specified for each particular system size and were chosen to ensure the best visual presentation of the entanglement entropy plots. While our construction guarantees the presence of many-body scars in any dimension and is insensitive to the boundary conditions we perform the numerical calculations in 1D and use open boundary conditions.

Given a Hamiltonian we perform full exact diagonalization obtaining the values for all the eigenvalues and eigenvectors. As the first test we examine the dimension of the $SO(N)$-singlet subspace. To do this we scale the part $(T_M + H_{\text{SB}})$ of the Hamiltonian (74) that is proportional to $SO(N)$ generators. Then we count the number of the energy levels that remain unchanged up to numerical precision. The number of these states is given in the Table I for several system sizes and agrees with the number of $SO(N)$ singlets given in Eq. (34).

The many-body scars are expected to stand out by violating the eigenstate thermalisation hypothesis in that an observable measured in these states clearly deviates from the thermal average at the same energy or temperature. We use entanglement entropy as one of the observables of interest.

In addition to the entanglement entropy we will also study the statistics of the level spacings in the spectrum. Going through the full spectrum we determine the level spacing and

TABLE I. The number of states in spectrum identified as many-body scars and the number of degenerate scar states.

N	M	Scars	Degenerate scars
2	12	924	380
3	12	8448	6144
4	6	70	0
4	8	588	204
6	6	168	0
8	4	18	0
9	4	20	0

level spacing ratio,

$$ s_i = E_i - E_{i-1}, \quad r_i = \frac{\min(s_i, s_{i+1})}{\max(s_i, s_{i+1})}, \tag{75} $$

for every pair of energy levels.

Mean values for this level spacing ratio is known analytically [66] for certain types of random matrices: $\langle r \rangle \approx 0.5359$ for the generalized orthogonal ensemble (GOE, real matrices) and $\langle r \rangle \approx 0.6027$ for the generalized unitary ensemble (GUE, complex matrices).

A. $M = 4$

The $M = 4$ case discussed in Sec. II has the same Hilbert space as the spin-1/2 electron models studied in Refs. [22,32].

We study numerically the system with $N = 8$, $M = 4$ and set $\mu_1 = 0.94854$, $\mu_2 = 0.14631$, $U = 0.72431$. The strength of the three-body symmetry-breaking term (23) is $p = 1.25196$. Note that the model we are studying with $M = 4$ reduces to the standard Hubbard model on identification $\mu_\uparrow = \mu_1 + \frac{U}{2}$; $\mu_\downarrow = \mu_2 + \frac{U}{2}$ and the energies of all the scars are specified at the end of Sec. II.

The entanglement entropy in the full Hilbert space and the level spacing histogram in the even sector of the fermion number parity (18) are shown in Fig. 1. Both families of scars have the entanglement entropy significantly lower than the generic states at the same temperature. Two states ($m = 0$ and $m = N$) in each scar family are product states and have exactly zero entanglement entropy.

Level spacings are analyzed in the even sector of the fermionic number parity, they are qualitatively the same in the odd sector. The average ratio of $\langle r \rangle \approx 0.59949$ we obtain is very close to the GUE value. The histogram of level spacings (excluding the singlet energy levels) shown in the bottom panel of Fig. 1 shows that the near-zero gaps are almost absent in the spectrum as is expected due to level repulsion and absence of residual symmetries. Altogether, we observe a chaotic bulk spectrum and the singlet states clearly violating ETH; this confirms that the singlet states are the many-body scars in this system.

B. $M > 4$

The first example we consider with $M > 4$ is $N = 4$, $M = 6$ for which a number of results are obtained analytically in Sec. IV D. We use the chemical potentials $\mu_1 = 5.69123$,
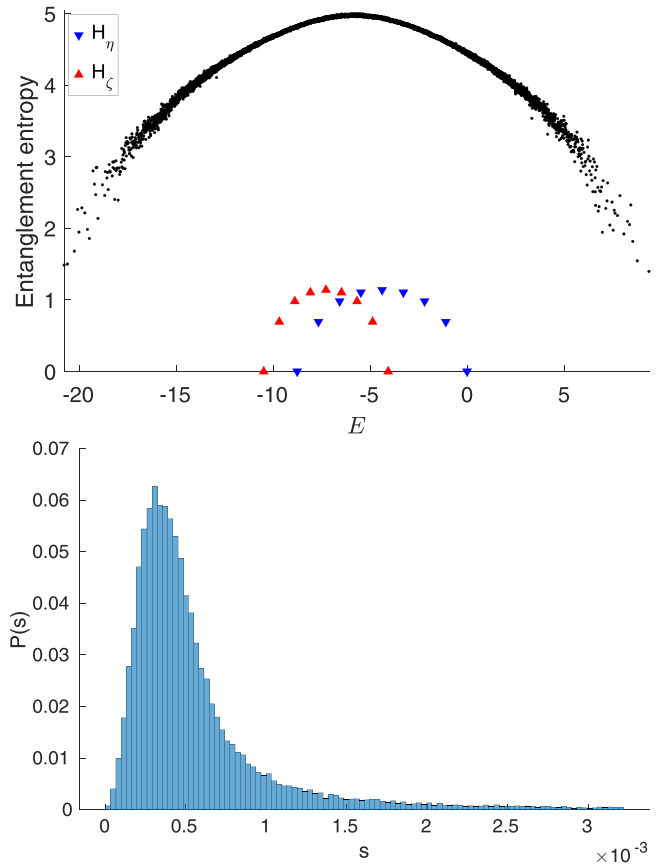

FIG. 1. Numerical results for $N = 8$, $M = 4$. Top panel: Entanglement entropy in every eigenstate in the sector with even fermion number, with the cut made in the middle of the 1D lattice. The η states are shown in blue, and the ζ states in red. Bottom panel: Probability for the level spacings in the even sector. We excluded 3% of largest gaps from the plot and from the total norm.

$\mu_2 = 0.87786$, $\mu_3 = 2.50648$, and $U = 2.89722$. The strength of the three-body term (23) is $p = 0.62598$.

The entanglement entropy in every eigenstate of the system is shown in Fig. 2. Together with the chaos properties of the bulk spectrum (not shown) it confirms the presence of many-body scars. An interesting property rarely observed in literature [24,37] and also seen in the next example is that the scars are not equidistant in energy while the Hamiltonian (74) we are studying is purely local.

Our main multiflavor example is $N = 4$, $M = 8$ where we use $\mu_1 = 5.69123$, $\mu_2 = 0.87786$, $\mu_3 = 2.50648$, $\mu_4 = 4.92193$, and $U = 2.89722$. The strength of the two-body symmetry-breaking term (26) is $p = 0.62598$.

The entanglement entropy in every eigenstate in the even fermion parity sector is shown in the top panel of Fig. 3. All the 588 SO(N) singlets 204 of which are (unbreakably) degenerate (64 triple-degenerate and 2 sixfold degenerate) are significantly less entangled than the generic states at the same temperature.

The average level spacing ratio in the even sector of the fermion number parity is 0.59715 and is approximately the same as the reference value for Hermitian random matrices (GUE). Vanishing probability of near-zero gaps that can be
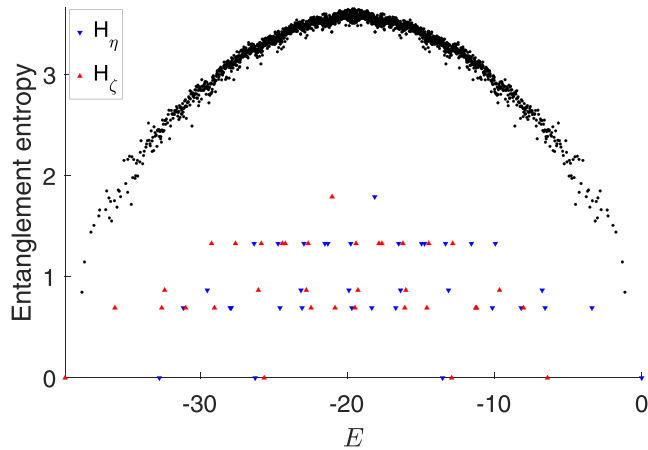
FIG. 2. Entanglement entropy plot for $N = 4$, $M = 6$ in the even fermion parity sector. The η states are shown in blue, and the ζ states in red.

seen in the bottom panel of Fig. 3 indicates level repulsion characteristic of ergodic quantum systems without symmetries. Combining these observations we can conclude that also in the $M > 4$ case the SO(N) singlets have all the properties of the many-body scars. We note that with the choice of "random" μ_α we made, the system in question has scars [their energy given in Eq. (39)] that are not equally spaced in energy. The off-diagonal long-range order [Eq. (61)] measured between the most distant sites ($i = 1$, $j = 4$) for $A = 1$ and $B = 2$ is shown in Fig. 4. As predicted by the Eq. (65) the sum of $M = O_{14}^{AB}$ measured in all the scar states normalized by the dimension of the scar subspace equals $\frac{1}{28}$ and is independent of the choice of A and B. We confirm numerically that the full minimal set of the ODLRO measurements contains $M - 1$ operators (61) where A and B are chosen as $(k, k + 1)$ for k between 1 and $M - 1$. This means that at least one of the $M - 1$ correlators is nonzero in every scar state.

Because of their controlled and predictable values in scars the ODLRO measurements can be used in experiment for detecting invariant many-body scars as an alternative to tracking the projection of the wave function on the scar subspace.

VII. ERGODICITY BREAKING IN NONLOCAL MODELS

The many-body scars reported in the literature so far are typically equidistant in energy. Such scars form an integrable subspace. We will now consider an H_0 that is nonlocal and nonintegrable by adding the term (42) that introduces a strong interaction within the scar subspace. We show that, in this situation, the scar singlets become fully chaotic and ergodic while remaining decoupled from the bulk spectrum.

We investigate the system with $N = 4$ and $M = 8$ and set the parameters identical to those used for obtaining Figs. 3 and 4 but add also the term in Eq. (42) with the coefficient 0.62598 and the random numbers r_{ABCD} drawn uniformly between 0 and 1. This additional term is second order in the generators of SO(M). It respects the SO(N) symmetry and is, therefore, of the H_0 type. It leaves the scar subspace invariant but mixes up
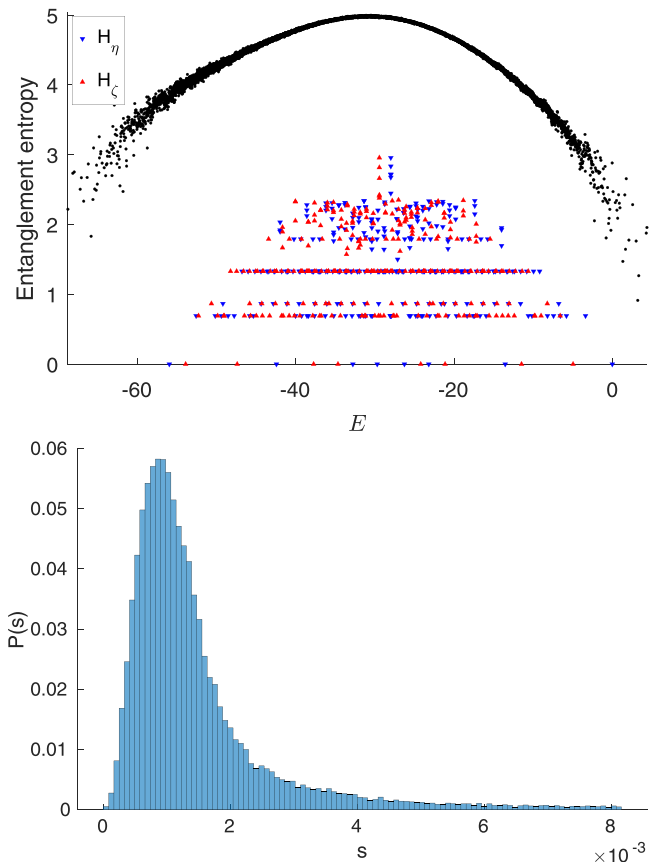

FIG. 3. Numerical results for $N = 4$, $M = 8$. Top panel: Entanglement entropy plot for the even sector, with the cut made in the middle of the 1D lattice. There are 16 nondegenerate product scar states with $S = 0$ (8 in the η sector and 8 in the ζ sector). Bottom panel: Probability of a level spacing in the even sector of the spectrum. We exclude 3% of largest gaps from the plot and from the total norm.

the scars [SO(N) singlets] and is, therefore, able to generate ergodic spectrum within the scar subspace. Let us also recall that (42) breaks the "unbreakable degeneracies" of the singlet states as discussed in Sec. IV B.
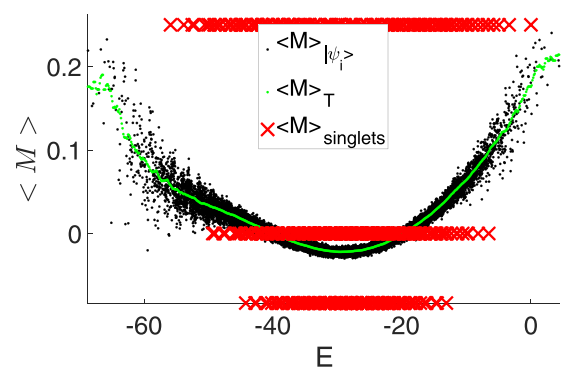

FIG. 4. The off-diagonal long-range order (61) with $M = O_{14}^{12}$; measured in every eigenstate (black dots) and in the SO(N)-singlet scar states (red crosses). The green line is the microcanonical (window) average.
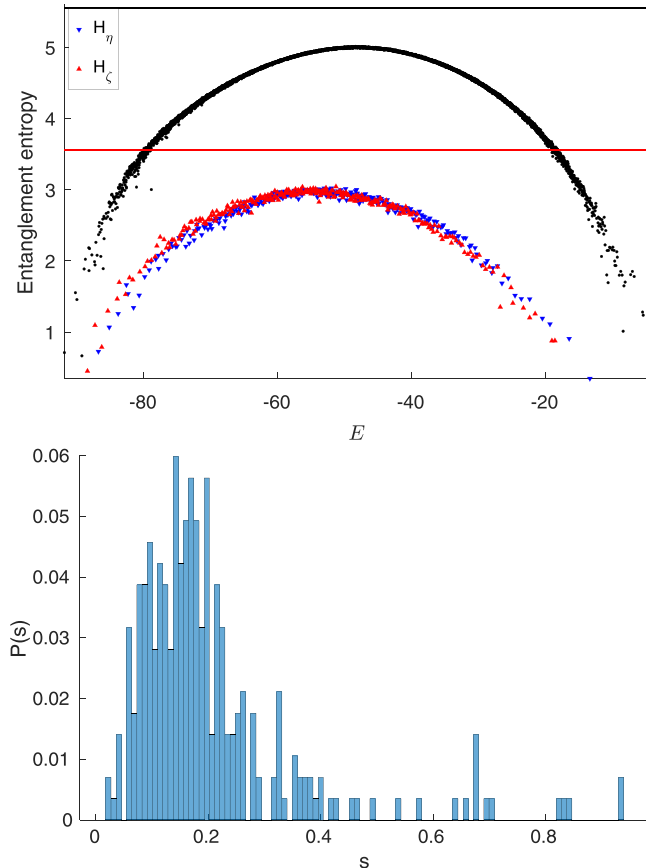
FIG. 5. Top panel: Entanglement entropy in the even fermionic parity sector for $N = 4$, $M = 8$ for the Hamiltonian including the scar-mixing term (42). The horizontal lines indicate the bounds on entanglement for a generic and a scar state according to Eq. (69). Bottom panel: The level spacing histogram for the 294 states in the $\mathcal{H}_\eta$ part of the scar subspace; 3% of the largest gaps are excluded.

The resulting entanglement entropies are shown in the top panel of Fig. 5. The entropies in the scar subspace form a nice thermal arc similarly to the generic states but separate from the original thermal arc. Note that the entanglement entropy calculation (C6) does not apply here because it was performed for the scar wave functions that are eigenstates of the simple integrable H_0 included in Eq. (74). Nonetheless, the entanglement entropy should and does satisfy the general bound (69) shown as the red horizontal line.

In the bottom panel of Fig. 5 we show the histogram of the level spacings within the $\mathcal{H}_\eta$ half of the scar subspace. In spite of the relatively small size of the subspace (294 states), we can see the emergence of the GUE profile (see also the data for a larger system in Fig. 7) with the near-zero gaps being almost absent—an expected signature consequence of level repulsion in an ergodic system without remaining symmetries. The average level statistics ratio $\langle r \rangle_\eta = 0.61801$ [see Eq. (75)] confirms that the level spacing belongs to the GUE. The level spacing behavior for $\mathcal{H}_\zeta$ half of the scar subspace (not shown) that is related to $\mathcal{H}_\eta$ by a symmetry transformation also appears ergodic. The average level spacing there is $\langle r \rangle_\zeta = 0.60764$.

VIII. ENHANCING THE SCAR CONTRIBUTION TO THE DENSITY OF STATES

We now turn to the interesting effects that the scar states in multiband systems can have on the density of states (DOS). Usually, in the limit of large system size, the scar states form a subspace of measure zero. Therefore, they would not be noticeable in the DOS. This is different in small multiband systems where a scar subspace can occupy a sizable fraction of the full Hilbert space. In the two cases $N = 2$, $M = 16$ and $N = 3$, $M = 12$ that we investigate numerically, the portion of scars is 39% and 3.2%. This means that, depending on the position of the scar states in energy (that can in principle be controlled, see Sec. III B) the scar states will strongly affect the DOS and could therefore be experimentally detectable.

Figure 6 shows the density of states with the scars contribution indicated separately for the systems with $N = 2$, $M = 16$ and $N = 3$, $M = 12$. Scars make a significant effect on the shape of the DOS in certain energy ranges (we do, however, expect this effect to weaken if we increase N while keeping M fixed). Using the term (29) the scars can also be localized near the low-energy part of the spectrum. The prevalence of scars in DOS could be seen in any measurement made at the corresponding temperature. This greatly simplifies the experimental studies of scars eliminating the need to prepare a specific initial state of the system. We emphasize that in all the cases presented in Fig. 6 the full Hamiltonian is local. Further possibilities of engineering the shape of the DOS are illustrated in the Fig. 8 in the Appendix.

The dimension of the scar subspace (35) quickly grows with N and M. The full Hilbert space dimension, however, grows even faster. Therefore the exotic signatures of scars in the DOS can only be observed in small systems. If we qualitatively set a 0.1% threshold on the fraction of the scars in the Hilbert space, then the largest suitable systems are $(N, M) : (6, 6), (4, 24), (3, 40)$. While small from the real material perspective they may be well suited for the existing quantum simulators based on cold atoms or quantum computing devices.

IX. DISCUSSION

We have presented the structure of the quantum many-body scars in lattice systems of N sites with M Majorana fermions per site. Following the idea of group-invariant scars [22,32] we identified the classes of ergodic Hamiltonians where the SO(N)-invariant states are exact eigenstates and many-body scars. Analytical expressions for the energies of scars and their signature off-diagonal long-range order correlators are provided. We specify how the scar wave functions can be built for arbitrary M and provide their explicit wave functions for $M = 6$. Some of these generalized η-pairing states were found also in Ref. [43].

The upper bound on the entanglement entropy of scars is derived for arbitrary M. It grows logarithmically with the subsystem size, generalizing the earlier results for $M = 4$ [10] and $M = 6$ [43]. Furthermore, we obtain an upper bound on the entanglement entropy for any group-invariant states, not limited to the multiflavor Majorana Hilbert spaces considered in this work. This leads us to a general conclusion
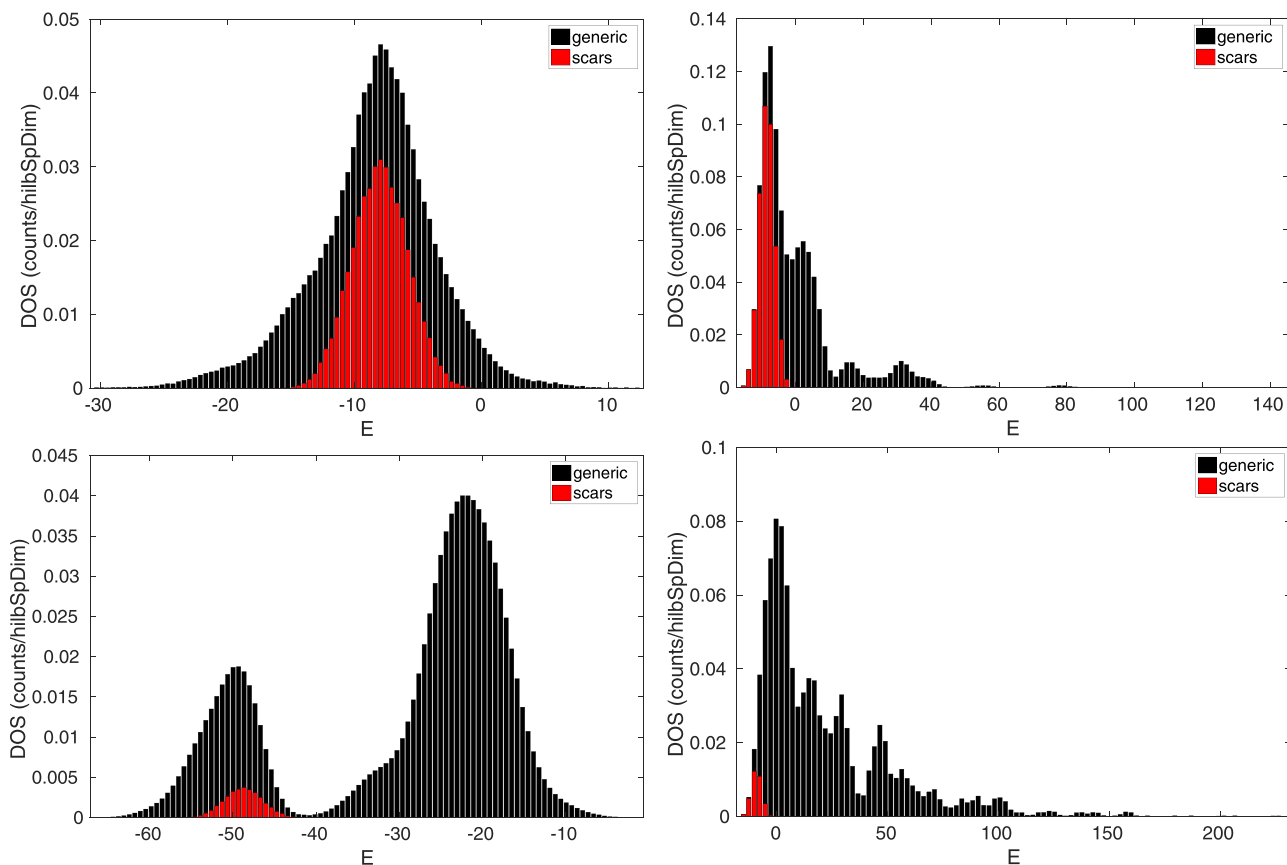
FIG. 6. The density of states where the contribution of scars in every energy window is shown in red. The Hamiltonian is (74) and the parameters are the same as in Fig. 3 except that all the chemical potentials are scaled down by a factor of 2/9. Further modifications are indicated below. Top: $N = 2$, $M = 16$, even fermionic parity sector (contains both η and ζ scars because N is even). Top left: No further modifications to the Hamiltonian. Top right: The positive-definite local term (29) with the coefficient 4.52691 is added. Bottom: $N = 3$, $M = 12$. The DOS is shown in the odd fermionic parity sector (contains only the ζ scars because N is odd). Bottom left: The Hamiltonian is modified by scaling up the U interaction term by a factor of 150. Bottom right: The term (29) is added with the strength of 9.05382.

that any group-invariant many-body scars must always have the entanglement entropy that is parametrically lower than that of generic states. This is in agreement with the calculations in almost all models with many-body scars, where

the general argument for the reduced entropy has not been provided yet.

The Hilbert space of multiflavor Majorana fermions used in this work allowed us to uncover several possibilities for the
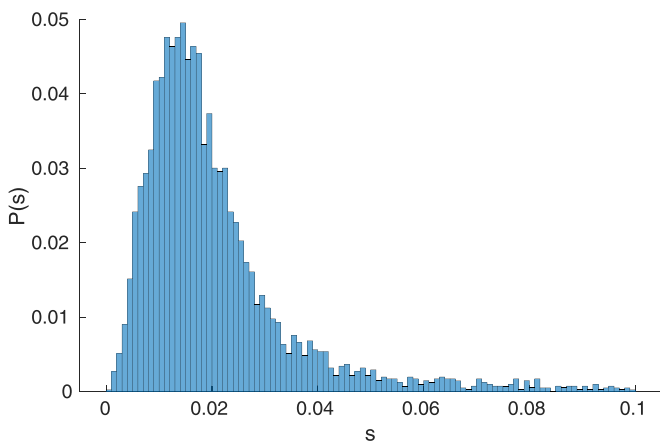

FIG. 7. $N = 3$, $M = 12$. Histogram of the energy gaps within the $\mathcal{H}_\eta$ subspace in even fermion parity sector; 3% of largest gaps excluded.
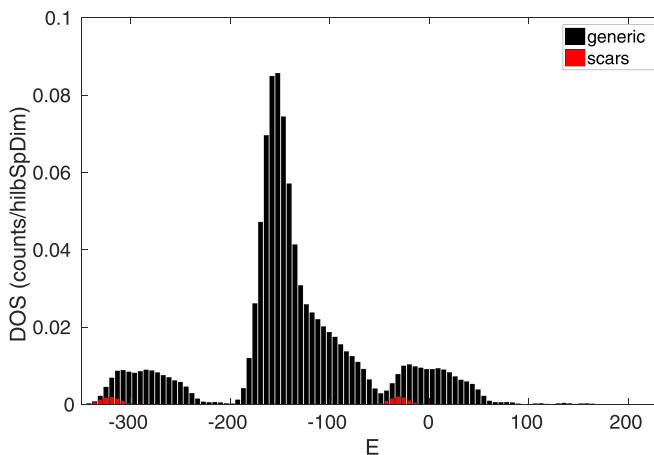

FIG. 8. $N = 4$, $M = 8$. Even fermionic parity sector. Hamiltonian is the same as in Fig. 3 but the U interaction term is scaled up by a factor of 200 and the positive-definite term (29) is added with strength 11.31727.

behavior of scars that were not discussed in the earlier literature. The number of states breaking ergodicity in a system with N sites and M flavors grows as $N^{M(M-2)/8}$. This means that for some system sizes the scars can occupy a sizable fraction of the Hilbert space and can be clearly seen in the density of states. For $M > 6$ we find degeneracies in the scar subspace that cannot be lifted by the local interactions which preserve the decoupling of scars. These degeneracies present a new promising resource that could potentially be used for robust quantum computing, similarly to how the topological degeneracies are used in topological quantum computing schemes [67].

Although the many-body scars we study can exhibit revivals under some conditions, they are not in general equally spaced in energy. Further, we demonstrated that by considering a nonlocal interaction the spectrum of scars can be made ergodic. It is an interesting question for the future studies if this requirement applies to all many-body scars in general. Should systems with ergodic scars be implemented in local systems, the experimental consequences of the simultaneous presence of two distinct thermal averages (as in Fig. 5) is another intriguing direction.

Finally, the models with multiple Majorana flavors possess a rich variety of the off-diagonal long-range order two-point correlators. The result of measuring such correlators in a scar state does not depend on the distance between the points. Similarly to the superconducting correlations found in the η states for $M = 4$, the full set of the corresponding ODLRO operators we identified for $M > 4$, may be used for detecting many-body scars experimentally.

APPENDIX A: A BRIEF REVIEW OF $\mathfrak{so}(2n, \mathbb{C})$ AND ITS REPRESENTATIONS

The complexified Lie algebra $\mathfrak{so}(2n, \mathbb{C})$ are spanned by all antisymmetric matrices over $\mathbb{C}$. A convenient basis of $\mathfrak{so}(2n, \mathbb{C})$ is given by

$$J^{AB} = E^{AB} - E^{BA}, \quad (E^{AB})_{CD} = \delta^A_C \delta^B_D, \quad \text{(A1)}$$

where E^{AB} is an $2n \times 2n$ matrix with only one nonzero entry. J^{AB} constructed in this way satisfy the commutation relation (13), and they are realized as anti-Hermitian operators acting on certain Hilbert space in a unitary representation. The

standard definition of quadratic Casimir is

$$\mathcal{C}_2^{\mathrm{SO}(2n)} = \frac{1}{2} \sum_{A,B=1}^{2n} J^{AB} J^{BA}. \quad \text{(A2)}$$

We choose Cartan generators to be

$$h_\alpha = -i J^{2\alpha-1, 2\alpha}, \quad \alpha = 1, 2, \ldots, n \quad \text{(A3)}$$

and they span a Cartan subalgebra $\mathfrak{h}$. Given this choice of Cartan subalgebra, positive roots are $e_\alpha \pm e_\beta, \quad 1 \leqslant \alpha < \beta \leqslant n$, with $\{e_\alpha\}$ being the standard basis on $\mathbb{R}^n$. The corresponding $\mathrm{SO}(2n)$ generators are

$$e_\alpha - e_\beta : \zeta^\dagger_{\alpha\beta}$$
$$= \frac{J^{2\alpha-1,2\beta-1} - i J^{2\alpha-1,2\beta} + i(J^{2\alpha,2\beta-1} - i J^{2\alpha,2\beta})}{2}$$

$$e_\alpha + e_\beta : \eta^\dagger_{\alpha\beta}$$
$$= \frac{J^{2\alpha-1,2\beta-1} + i J^{2\alpha-1,2\beta} + i(J^{2\alpha,2\beta-1} + i J^{2\alpha,2\beta})}{2}, \quad \text{(A4)}$$

where the overall normalization factor $\frac{1}{2}$ is inserted such that $[\zeta^\dagger_{\alpha\beta}, \eta^\dagger_{\beta\gamma}] = \eta^\dagger_{\alpha\gamma}$. The generators corresponding to negative roots $-(e_\alpha \pm e_\beta)$ are Hermitian conjugate of $\zeta^\dagger_{\alpha\beta}$ and $\eta^\dagger_{\alpha\beta}$. Altogether, the root decomposition of $\mathfrak{so}(2n, \mathbb{C})$ is

$$\mathfrak{so}(2n, \mathbb{C}) = \mathfrak{h} \bigoplus \bigoplus_{1 \leqslant \alpha < \beta \leqslant n} (\mathbb{C}\zeta^\dagger_{\alpha\beta} \oplus \mathbb{C}\eta^\dagger_{\alpha\beta} \oplus \mathbb{C}\zeta_{\alpha\beta} \oplus \mathbb{C}\eta_{\alpha\beta}).$$

$$\text{(A5)}$$

An integral highest-weight vector λ can be parameterized by $\lambda = \sum_{\alpha=1}^n \lambda_\alpha e_\alpha$, where λ_α are either integers or half-integers, satisfying $\lambda_1 \geqslant \lambda_2 \geqslant \cdots \geqslant \lambda_{n-1} \geqslant |\lambda_n|$. In terms of Young diagram, λ_α is the number of boxes in the αth row. Given a highest-weight vector $\lambda = (\lambda_1, \cdots, \lambda_n)$, the Casimir $\mathcal{C}_2^{\mathrm{SO}(2n)}$ defined by Eq. (A2) takes the value

$$\mathcal{C}_2^{\mathrm{SO}(2n)}(\lambda) = \sum_{\alpha=1}^n \lambda_\alpha(\lambda_\alpha + 2n - 2\alpha), \quad \text{(A6)}$$

which cannot be used to distinguish the two highest-weight representations $(\lambda_1, \cdots, \pm\lambda_n)$. For a rectangular Young diagram $\lambda = (k^n)$ (k is an arbitrary non-negative integer), Eq. (A6) yields

$$\mathcal{C}_2^{\mathrm{SO}(2n)}(k^n) = \mathcal{C}_2^{\mathrm{SO}(2k)}(n^k) = kn(n + k - 1). \quad \text{(A7)}$$

The Weyl character of the λ representation, defined as the trace of $x_1^{h_1} \cdots x_n^{h_n}$ over the Hilbert space, is given by

$$\chi_\lambda^{\mathrm{SO}(2n)}(\boldsymbol{x}) = \frac{\det\left(x_\alpha^{\ell_\beta} + x_\alpha^{-\ell_\beta}\right) + \det\left(x_\alpha^{\ell_\beta} - x_\alpha^{-\ell_\beta}\right)}{\det\left(x_\alpha^{n-\beta} + x_\alpha^{-(n-\beta)}\right)}, \quad \text{(A8)}$$

where $\ell_\alpha = n + \lambda_\alpha - \alpha$. Taking the $x_\alpha \to 1$ limit in $\chi_\lambda^{\mathrm{SO}(2n)}(\boldsymbol{x})$ yields the dimension of this representation

$$\dim_\lambda^{\mathrm{SO}(2n)} = \prod_{\alpha < \beta} \frac{(\ell_\alpha - \ell_\beta)(\ell_\alpha + \ell_\beta)}{(\beta - \alpha)(2n - \alpha - \beta)}. \quad \text{(A9)}$$

APPENDIX B: ADDITIONAL NUMERICAL RESULTS

Figure 7 shows the distribution of the energy gaps in the scar subspace for the model parameters that are identical to those used for Fig. 5 but in a larger system with 4224 η scars. The average level statistics ratio here is $\langle r \rangle_\eta = 0.59335$ and $\langle r \rangle_\zeta = 0.60095$ for the ζ states (histogram is qualitatively the same but not shown). As in the main text the data are fully consistent with an ergodic spectrum without remaining symmetries also within the scar subspace.

Figure 8 illustrates that by combining the stronger U interaction and the positive-definite term (29) the scars can be exposed even in the DOS of the systems where they only occupy a vanishingly small part of the Hilbert space.

APPENDIX C: ENTANGLEMENT ENTROPY FOR $M = 6$

Using the explicit expression (49) for all the η states in the $M = 6$ case, we can calculate their entanglement entropy analytically. We divide the underlying lattice into two disjoint subsets Σ_1 and Σ_2. For example, Σ_1 consists of the first N_1 sites, i.e., $i = 1, 2, \ldots, N_1$, and Σ_2 consists of the rest $N_2 = N - N_1$ sites. In each sublattice Σ_a, there is an empty vacuum $|0\rangle_a$ satisfying $|0\rangle = |0\rangle_1 \otimes |0\rangle_2$. Then we are allowed to split the η-operators in the following way:

$$\eta_{\alpha\beta}^{1\dagger} = \sum_{i=1}^{N_1} c_{i\alpha}^\dagger c_{i\beta}^\dagger, \quad \eta_{\alpha\beta}^{2\dagger} = \sum_{i=N_1+1}^{N} c_{i\alpha}^\dagger c_{i\beta}^\dagger,$$

such that $\eta_{\alpha\beta}^{a\dagger}$ can excite η states of the subsystem Σ_a on $|0\rangle_a$,

$$|m_{12}, m_{13}, m_{23}\rangle_a = C_{\boldsymbol{m}}(N_a) \prod_{\alpha<\beta} \left(\eta_{\alpha\beta}^{a\dagger}\right)^{m_{\alpha\beta}} |0\rangle_a. \quad \text{(C1)}$$

Because of $\eta_{\alpha\beta}^\dagger = \eta_{\alpha\beta}^{1\dagger} + \eta_{\alpha\beta}^{2\dagger}$, we have a tensor product decomposition of any η state $|\boldsymbol{k}\rangle \equiv |k_{12}, k_{13}, k_{23}\rangle$ defined in Eq. (49),

$$|\boldsymbol{k}\rangle = C_{\boldsymbol{k}}(N) \sum_{m_{\alpha\beta}=0}^{k_{\alpha\beta}} \prod_{\alpha<\beta} \binom{k_{\alpha\beta}}{m_{\alpha\beta}} \left(\eta_{\alpha\beta}^{1\dagger}\right)^{m_{\alpha\beta}} \left(\eta_{\alpha\beta}^{2\dagger}\right)^{k_{\alpha\beta}-m_{\alpha\beta}} |0\rangle$$

$$= \sum_{m_{\alpha\beta}=0}^{k_{\alpha\beta}} \frac{C_{\boldsymbol{k}}(N)}{C_{\boldsymbol{m}}(N_1) C_{\boldsymbol{k}-\boldsymbol{m}}(N_2)} \prod_{\alpha<\beta} \binom{k_{\alpha\beta}}{m_{\alpha\beta}} |\boldsymbol{m}\rangle_1 \otimes |\boldsymbol{k}-\boldsymbol{m}\rangle_2.$$

Let us note that $|\boldsymbol{m}\rangle_1$ and $|\boldsymbol{k}-\boldsymbol{m}\rangle_2$ are also singlet states in each subsector. Taking the partial trace over the Hilbert space of Σ_2 yields the reduced density matrix $\rho_{\Sigma_1}(\boldsymbol{k})$ of $|\boldsymbol{k}\rangle$,

$$\rho_{\Sigma_1}(\boldsymbol{k}) = \sum_{m_{\alpha\beta}=0}^{k_{\alpha\beta}} \lambda_{\boldsymbol{k}}(\boldsymbol{m}) |\boldsymbol{m}\rangle_1 \langle \boldsymbol{m}|_1, \quad \text{(C2)}$$

where

$$\lambda_{\boldsymbol{k}}(\boldsymbol{m}) = \frac{C_{m_{12},m_{13},m_{23}}^{N_1} C_{k_{12}-m_{12},k_{13}-m_{13},k_{23}-m_{23}}^{N_2}}{C_{k_{12},k_{13},k_{23}}^{N}}$$

$$C_{a,b,c}^{N} \equiv \frac{N!}{a!\, b!\, c!\, (N-a-b-c)!}, \quad \text{(C3)}$$

and $\lambda_{\boldsymbol{k}}(\boldsymbol{m})$ vanishes when $m_T > N_1$ or $k_T - m_T > N_2$. The density matrix ρ_{Σ_1} corresponds to a pure state if (i) all $k_{\alpha\beta}$ are vanishing or (ii) one $k_{\alpha\beta}$ is equal to N and the rest are vanishing. The former is trivial since it implies $m_{12} = m_{13} = m_{23} = 0$. For the latter, say, $k_{12} = N$, we have first $m_{13} = m_{23} = 0$. Then nonvanishing $\lambda_{\boldsymbol{k}}(\boldsymbol{m})$ requires $m_T \geqslant k_T - N_2 = N_1$ and $m_T \leqslant N_1$, which completely fix $m_{12} = N_1$. Indeed, (i) corresponds to $|0\rangle$, and (ii) corresponds to $\mathcal{A}_\alpha^\dagger \mathcal{A}_\beta^\dagger |0\rangle$, $1 \leqslant \alpha < \beta \leqslant 3$, which are the only product states in $\mathcal{H}_\eta$.

Next we proceed to compute the entanglement entropy of $\rho_{\Sigma_1}(\boldsymbol{k})$ in the thermodynamic limit, defined as the limit of $N \to \infty$, $k_{\alpha\beta} \to \infty$ such that $\nu_{\alpha\beta} \equiv \frac{k_{\alpha\beta}}{N}$ are finite. We further choose $N_1 \ll N$ so that Σ_2 can be treated as a heat bath and meanwhile keep $N_1 \gg 1$ to allow scaling of entanglement entropy ρ_{Σ_1}. In this limit, $\lambda_{\boldsymbol{k}}(\boldsymbol{m})$ is sharply peaked around $m_{\alpha\beta} = m_{\alpha\beta}^* \equiv \nu_{\alpha\beta} N_1$. At this extremal point, $\lambda(\boldsymbol{m}^*) \approx \frac{1}{\sqrt{(2\pi N_1)^3 \nu_{12}\nu_{13}\nu_{23}(1-\nu_T)}}$ with $\nu_T = \nu_{12} + \nu_{13} + \nu_{23}$. For general $\boldsymbol{m}$, the matrix element $\lambda(\boldsymbol{m})$ is approximated by a 3D Gaussian centered at $\boldsymbol{m}^*$,

$$\lambda(\boldsymbol{m}) \approx \frac{e^{-\frac{1}{2N_1}(\boldsymbol{m}-\boldsymbol{m}^*)^T \mathcal{M}(\boldsymbol{m}-\boldsymbol{m}^*)}}{\sqrt{(2\pi N_1)^3 \nu_{12}\nu_{13}\nu_{23}(1-\nu_T)}}, \quad \text{(C4)}$$

where $\mathcal{M}$ is a 3×3 symmetric matrix, given by

$$\mathcal{M} = \begin{pmatrix} \frac{1}{\nu_{12}} + \frac{1}{1-\nu_T} & \frac{1}{1-\nu_T} & \frac{1}{1-\nu_T} \\ \frac{1}{1-\nu_T} & \frac{1}{\nu_{13}} + \frac{1}{1-\nu_T} & \frac{1}{1-\nu_T} \\ \frac{1}{1-\nu_T} & \frac{1}{1-\nu_T} & \frac{1}{\nu_{23}} + \frac{1}{1-\nu_T} \end{pmatrix} \quad \text{(C5)}$$

with determinant equal to $\nu_{12}\nu_{13}\nu_{23}(1-\nu_T)$. The scaling property of the entanglement entropy of $\rho_{\Sigma_1}(\boldsymbol{k})$ in thermodynamic limit can then be computed by replacing the sum over $\boldsymbol{m}$ with a triple integral $\int d^3\boldsymbol{m}$:

$$S_{\Sigma_1}(\boldsymbol{k}) \approx - \int d^3\boldsymbol{m} \, \lambda_{\boldsymbol{k}}(\boldsymbol{m}) \log \lambda_{\boldsymbol{k}}(\boldsymbol{m})$$

$$\approx \frac{1}{2} \log((2\pi N_1)^3 \nu_{12}\nu_{13}\nu_{23}(1-\nu_T)) \sim \frac{3}{2} \log(N_1) \quad \text{(C6)}$$

The calculation of entanglement entropy works analogously for the other $SO(N)$-invariant subspace $\mathcal{H}_\zeta$. In particular, starting with a ζ state $|\boldsymbol{k}\rangle^\zeta$, we end up with same density matrix (C2), with $|\boldsymbol{m}\rangle_1$ being replaced by the corresponding ζ states on Σ_1.

[1] C. J. Turner, A. A. Michailidis, D. A. Abanin, M. Serbyn, and Z. Papić, Weak ergodicity breaking from quantum many-body scars, Nat. Phys. **14**, 745 (2018).

[2] I. Lesanovsky and H. Katsura, Interacting fibonacci anyons in a Rydberg gas, Phys. Rev. A **86**, 041601(R) (2012).

[3] N. Shiraishi and T. Mori, Systematic construction of counterexamples to the eigenstate thermalization hypothesis, Phys. Rev. Lett. **119**, 030601 (2017).

[4] S. Moudgalya, N. Regnault, and B. A. Bernevig, Entanglement of exact excited states of Affleck-Kennedy-Lieb-Tasaki models:

Exact results, many-body scars, and violation of the strong eigenstate thermalization hypothesis, Phys. Rev. B **98**, 235156 (2018).

[5] S. Choi, C. J. Turner, H. Pichler, W. W. Ho, A. A. Michailidis, Z. Papić, M. Serbyn, M. D. Lukin, and D. A. Abanin, Emergent SU(2) dynamics and perfect quantum many-body scars, Phys. Rev. Lett. **122**, 220603 (2019).

[6] V. Khemani, M. Hermele, and R. Nandkishore, Localization from Hilbert space shattering: From theory to physical realizations, Phys. Rev. B **101**, 174204 (2020).

[7] P. Sala, T. Rakovszky, R. Verresen, M. Knap, and F. Pollmann, Ergodicity breaking arising from Hilbert space fragmentation in dipole-conserving hamiltonians, Phys. Rev. X **10**, 011047 (2020).

[8] S. Moudgalya, A. Prem, R. Nandkishore, N. Regnault, and B. A. Bernevig, Thermalization and its absence within Krylov subspaces of a constrained Hamiltonian, *Memorial Volume for Shoucheng Zhang* (World Scientific, Singapore, 2021), Chap. 7, pp. 147–209.

[9] M. Schecter and T. Iadecola, Weak ergodicity breaking and quantum many-body scars in spin-1 xy magnets, Phys. Rev. Lett. **123**, 147201 (2019).

[10] O. Vafek, N. Regnault, and B. A. Bernevig, Entanglement of exact excited eigenstates of the Hubbard model in arbitrary dimension, SciPost Phys. **3**, 043 (2017).

[11] T. Iadecola and M. Žnidarič, Exact localized and ballistic eigenstates in disordered chaotic spin ladders and the Fermi-Hubbard model, Phys. Rev. Lett. **123**, 036403 (2019).

[12] N. Shibata, N. Yoshioka, and H. Katsura, Onsager's scars in disordered spin chains, Phys. Rev. Lett. **124**, 180604 (2020).

[13] A. A. Michailidis, C. J. Turner, Z. Papić, D. A. Abanin, and M. Serbyn, Stabilizing two-dimensional quantum scars by deformation and synchronization, Phys. Rev. Res. **2**, 022065(R) (2020).

[14] D. K. Mark and O. I. Motrunich, η-pairing states as true scars in an extended Hubbard model, Phys. Rev. B **102**, 075132 (2020).

[15] K. Bull, I. Martin, and Z. Papić, Systematic construction of scarred many-body dynamics in 1D lattice models, Phys. Rev. Lett. **123**, 030601 (2019).

[16] V. Khemani, C. R. Laumann, and A. Chandran, Signatures of integrability in the dynamics of Rydberg-blockaded chains, Phys. Rev. B **99**, 161101(R) (2019).

[17] K. Lee, R. Melendrez, A. Pal, and H. J. Changlani, Exact three-colored quantum scars from geometric frustration, Phys. Rev. B **101**, 241111(R) (2020).

[18] D. K. Mark, C.-J. Lin, and O. I. Motrunich, Unified structure for exact towers of scar states in the Affleck-Kennedy-Lieb-Tasaki and other models, Phys. Rev. B **101**, 195131 (2020).

[19] T. Iadecola and M. Schecter, Quantum many-body scar states with emergent kinetic constraints and finite-entanglement revivals, Phys. Rev. B **101**, 024306 (2020).

[20] S. Moudgalya, N. Regnault, and B. A. Bernevig, η-pairing in Hubbard models: From spectrum generating algebras to quantum many-body scars, Phys. Rev. B **102**, 085140 (2020).

[21] B. van Voorden, J. C. V. Minář, and K. Schoutens, Quantum many-body scars in transverse field ising ladders and beyond, Phys. Rev. B **101**, 220305(R) (2020).

[22] K. Pakrouski, P. N. Pallegar, F. K. Popov, and I. R. Klebanov, Many-body scars as a group invariant sector of Hilbert space, Phys. Rev. Lett. **125**, 230602 (2020).

[23] J. Ren, C. Liang, and C. Fang, Quasisymmetry groups and many-body scar dynamics, Phys. Rev. Lett. **126**, 120604 (2021).

[24] N. O'Dea, F. Burnell, A. Chandran, and V. Khemani, From tunnels to towers: Quantum scars from lie algebras and q-deformed lie algebras, Phys. Rev. Res. **2**, 043305 (2020).

[25] N. S. Srivatsa, J. Wildeboer, A. Seidel, and A. E. B. Nielsen, Quantum many-body scars with chiral topological order in two dimensions and critical properties in one dimension, Phys. Rev. B **102**, 235106 (2020).

[26] C.-J. Lin, V. Calvera, and T. H. Hsieh, Quantum many-body scar states in two-dimensional Rydberg atom arrays, Phys. Rev. B **101**, 220304(R) (2020).

[27] S. Moudgalya, E. O'Brien, B. A. Bernevig, P. Fendley, and N. Regnault, Large classes of quantum scarred Hamiltonians from matrix product states, Phys. Rev. B **102**, 085120 (2020).

[28] K. Mizuta, K. Takasan, and N. Kawakami, Exact floquet quantum many-body scars under Rydberg blockade, Phys. Rev. Res. **2**, 033284 (2020).

[29] K. Bull, J.-Y. Desaules, and Z. Papić, Quantum scars as embeddings of weakly broken lie algebra representations, Phys. Rev. B **101**, 165139 (2020).

[30] Y. Kuno, T. Mizoguchi, and Y. Hatsugai, Multiple quantum scar states and emergent slow thermalization in a flat-band system, Phys. Rev. B **104**, 085130 (2021).

[31] D. Banerjee and A. Sen, Quantum scars from zero modes in an Abelian lattice gauge theory on ladders, Phys. Rev. Lett. **126**, 220601 (2021).

[32] K. Pakrouski, P. N. Pallegar, F. K. Popov, and I. R. Klebanov, Group theoretic approach to many-body scar states in fermionic lattice models, Phys. Rev. Res. **3**, 043156 (2021).

[33] S. Pilatowsky-Cameo, D. Villaseñor, M. A. Bastarrachea-Magnani, S. Lerma-Hernández, L. F. Santos, and J. G. Hirsch, Ubiquitous quantum scarring does not prevent ergodicity, Nat. Commun. **12**, 852 (2021).

[34] N. Maskara, A. A. Michailidis, W. W. Ho, D. Bluvstein, S. Choi, M. D. Lukin, and M. Serbyn, Discrete time-crystalline order enabled by quantum many-body scars: Entanglement steering via periodic driving, Phys. Rev. Lett. **127**, 090602 (2021).

[35] C. M. Langlett, Z.-C. Yang, J. Wildeboer, A. V. Gorshkov, T. Iadecola, and S. Xu, Rainbow scars: From area to volume law, Phys. Rev. B **105**, L060301 (2022).

[36] J. Ren, C. Liang, and C. Fang, Deformed symmetry structures and quantum many-body scar subspaces, Phys. Rev. Res. **4**, 013155 (2022).

[37] L.-H. Tang, N. O'Dea, and A. Chandran, Multimagnon quantum many-body scars from tensor operators, Phys. Rev. Res. **4**, 043006 (2022).

[38] H. Yoshida and H. Katsura, Exact eigenstates of extended SU(n) hubbard models: Generalization of η-pairing states with n-particle off-diagonal long-range order, Phys. Rev. B **105**, 024520 (2022).

[39] F. Schindler, N. Regnault, and B. A. Bernevig, Exact quantum scars in the chiral nonlinear Luttinger liquid, Phys. Rev. B **105**, 035146 (2022).

[40] G. Barnes, A. Padellaro, and S. Ramgoolam, Permutation symmetry in large-N matrix quantum mechanics and partition algebras, Phys. Rev. D **106**, 106020 (2022).

[41] S. Moudgalya and O. I. Motrunich, From symmetries to commutant algebras in standard Hamiltonians, Ann. Phys. **455**, 169384 (2023).

[42] S. Moudgalya and O. I. Motrunich, Exhaustive characterization of quantum many-body scars using commutant algebras, arXiv:2209.03377 [cond-mat.str-el] (2022).

[43] M. Nakagawa, H. Katsura, and M. Ueda, Exact eigenstates of multicomponent Hubbard models: SU(N) magnetic η pairing, weak ergodicity breaking, and partial integrability, arXiv:2205.07235 [cond-mat.str-el] (2022).

[44] L. Gotta, L. Mazza, P. Simon, and G. Roux, Exact many-body scars based on pairs or multimers in a chain of spinless fermions, Phys. Rev. B **106**, 235147 (2022).

[45] M. Dodelson and A. Zhiboedov, Gravitational orbits, double-twist mirage, and many-body scars, J. High Energy Phys. 12 (2022) 163.

[46] P. Caputa and D. Ge, Entanglement and geometry from subalgebras of the virasoro algebra, J. High Energy Phys. 06 (2023) 159.

[47] D. Liska, V. Gritsev, W. Vleeshouwers, and J. Minář, Holographic quantum scars, SciPost Phys. **15**, 106 (2023).

[48] B. Buča, J. Tindall, and D. Jaksch, Non-stationary coherent quantum many-body dynamics through dissipation, Nat. Commun. **10**, 1730 (2019).

[49] M. Serbyn, D. A. Abanin, and Z. Papić, Quantum many-body scars and weak breaking of ergodicity, Nat. Phys. **17**, 675 (2021).

[50] S. Moudgalya, B. A. Bernevig, and N. Regnault, Quantum many-body scars and Hilbert space fragmentation: A review of exact results, Rep. Prog. Phys. **85**, 086501 (2022).

[51] Z. Papić, Weak ergodicity breaking through the lens of quantum entanglement, in *Entanglement in Spin Chains: From Theory to Quantum Technology Applications*, edited by A. Bayat, S. Bose, and H. Johannesson (Springer International, Cham, 2022), pp. 341–395.

[52] A. Chandran, T. Iadecola, V. Khemani, and R. Moessner, Quantum many-body scars: A quasiparticle perspective, Annu. Rev. Condens. Matter Phys. **14**, 443 (2023).

[53] H. Alaeian and B. Buča, Exact multistability and dissipative time crystals in interacting fermionic lattices, Commun. Phys. **5**, 318 (2022).

[54] C. N. Yang, η pairing and off-diagonal long-range order in a Hubbard model, Phys. Rev. Lett. **63**, 2144 (1989).

[55] C. N. Yang and S. Zhang, So(4) symmetry in a Hubbard model, Mod. Phys. Lett. B **04**, 759 (1990).

[56] H. Zhai, Two generalizations of η pairing in extended Hubbard models, Phys. Rev. B **71**, 012512 (2005).

[57] B. Lian, Quantum breakdown model: From many-body localization to chaos with scars, Phys. Rev. B **107**, 115171 (2023).

[58] S. Zhang, So(4) symmetry of the Hubbard model and its experimental consequences, Int. J. Mod. Phys. B **05**, 153 (1991).

[59] H. Shiba, Thermodynamic properties of the one-dimensional half-filled-band Hubbard model. II: Application of the grand canonical method, Prog. Theor. Phys. **48**, 2171 (1972).

[60] F. H. L. Essler, H. Frahm, F. Goehmann, A. Kluemper, and V. E. Korepin, *The One-Dimensional Hubbard Model* (Cambridge University Press, Cambridge, UK, 2005).

[61] I. R. Klebanov, A. Milekhin, F. Popov, and G. Tarnopolsky, Spectra of eigenstates in fermionic tensor quantum mechanics, Phys. Rev. D **97**, 106023 (2018).

[62] G. Gaitan, I. R. Klebanov, K. Pakrouski, P. N. Pallegar, and F. K. Popov, Hagedorn temperature in large N majorana quantum mechanics, Phys. Rev. D **101**, 126002 (2020).

[63] C. Honerkamp and W. Hofstetter, Ultracold fermions and the SU(n) Hubbard model, Phys. Rev. Lett. **92**, 170403 (2004).

[64] J. E. Humphreys, *Introduction to Lie Algebras and Representation Theory*, Vol. 9 (Springer Science & Business Media, New York, 2012).

[65] Z. Yao, L. Pan, S. Liu, and P. Zhang, Bounding entanglement entropy using zeros of local correlation matrices, Phys. Rev. Res. **4**, L042037 (2022).

[66] Y. Y. Atas, E. Bogomolny, O. Giraud, and G. Roux, Distribution of the ratio of consecutive level spacings in random matrix ensembles, Phys. Rev. Lett. **110**, 084101 (2013).

[67] M. Freedman, A. Kitaev, M. Larsen, and Z. Wang, Topological quantum computation, Bull. Am. Math. Soc. **40**, 31 (2003).